The Astrophysical Journal, 599:1449–1468, 2003 December 20
© 2003. The American Astronomical Society. All rights reserved. Printed in U.S.A.

DYNAMO ACTION DRIVEN BY SHEAR AND MAGNETIC BUOYANCY

Kelly S. Cline and Nicholas H. Brummell
JILA and Department of Astrophysical and Planetary Sciences, University of Colorado, Boulder, CO 80309-0440

and

Fausto Cattaneo
Department of Mathematics, University of Chicago, 5734 South University Avenue, Chicago, IL 60637
Received 2003 June 16; accepted 2003 August 29

ABSTRACT

We present direct numerical simulations based on the full MHD equations of dynamo action in a non-rotating, convectively stable layer containing a forced, localized velocity shear. The dynamo operates by the interaction of two MHD processes: the production of toroidal magnetic field from poloidal field by the shear, and the regeneration of poloidal loops from toroidal field due to the combined action of magnetic buoyancy and Kelvin-Helmholtz instabilities. The nature of the dynamo process is such that it can occur only if the initial magnetic fields exceed a critical value that typically depends on the magnetic Reynolds number. As such, this dynamo does not operate in the kinematic limit. Several different behaviors are observed, including steady dynamo production and cyclic as well as chaotic activity. In the cyclic regimes, the dynamo process exhibits polarity reversals and periods of reduced activity.

Subject headings: MHD — stars: spots — Sun: interior — Sun: magnetic fields

1. INTRODUCTION

Solar active regions are believed to be the surface emergence points of toroidal magnetic structures that rise through the convective zone from deep within the Sun. The origin of this field is attributed to dynamo action operating within the solar interior (Moffatt 1978; Parker 1979; Krause & Rädler 1980). A number of basic processes are believed to play important roles in the generation mechanism. Differential rotation in both latitude and radius can wind poloidal magnetic field to produce toroidal field. This process is commonly referred to as the ω-effect in mean-field models of the solar dynamo (e.g., Steenbeck, Krause, & Rädler 1966). Helioseismology reveals that the strongest differential rotation is confined to a thin layer near the base of the convection zone (Goode et al. 1991; Thompson et al. 1996)—the tachocline (Spiegel 1972; Spiegel & Zahn 1992)—and it is commonly assumed that the ω-effect is concentrated within this region (see, e.g., Weiss 1994). Helical motions can convert toroidal field into poloidal field, thereby closing the dynamo feedback loop and allowing the magnetic field to grow. This process is referred to as the α-effect in mean-field theory. Its origin is not as well understood as that of the ω-effect and could be associated with the helical nature of the turbulent convection (Parker 1955b; Steenbeck & Krause 1969; Meneguzzi, Frisch, & Pouquet 1981; Brandenburg 2001) or the twisting of magnetic structures rising in a rotating environment (Babcock 1961; Leighton 1969; Ferriz-Mas, Schmitt, & Schüssler 1994; Brandenburg & Schmitt 1998; Thelen 2000; Dikpati & Gilman 2001).

Magnetic buoyancy (Parker 1955a), the tendency of magnetized fluid to be lighter than the unmagnetized surroundings and thus buoyant, also plays a part in the working of the solar dynamo. Although the origin of magnetic buoyancy is clear, arising simply from the requirement of continuity of total pressure across a magnetic structure, its role in the dynamo process is not straightforward. On the one hand, magnetic buoyancy provides a mechanism to limit the growth of the magnetic field by removing flux from the region of dynamo amplification. In this case, magnetic buoyancy instabilities control the dynamo amplitude but do not actively contribute to the workings of the generation process. On the other hand, if the α-effect is indeed associated with twisting of rising magnetic structures, then magnetic buoyancy is the very mechanism that drives the dynamo. In the former case, the dynamo operates *in spite* of magnetic buoyancy, whereas in the latter it operates *because* of magnetic buoyancy.

This dual role of magnetic buoyancy is often reflected in the way that its effects are incorporated into models of the solar dynamo. In mean-field models, magnetic buoyancy is sometimes included as a loss term typically proportional to the square of the field strength (Moss, Tuominen, & Brandenburg 1990); at other times, it is included as a driving term in the α-effect (Ferriz-Mas et al. 1994; Thelen 2000). In models based on the thin flux tube approximation (Defouw 1976; Spruit 1980), buoyancy effects are directly incorporated as one of the basic forces acting on the tubes. In all cases, however, the inclusion of magnetic buoyancy effects requires some a priori assumption as to the nature of their contribution.

In order better to understand the role of magnetic buoyancy in the dynamo process, we construct here a simple model that, although highly idealized, does not contain any presupposed assumptions or approximations. By basing this model on the solutions of the full MHD equations, we allow magnetic buoyancy to play whatever role it chooses. The model is a natural extension of that of Brummell, Cline, & Cattaneo (2002) and Cline, Brummell, & Cattaneo (2003, hereafter CBC) consisting of a stably stratified layer of conducting fluid in which a localized velocity shear is maintained. The shear provides a simple realization of the ω-effect generating a toroidal field from a poloidal one. The regeneration of the poloidal field to give rise to dynamo action proceeds through a complex interaction between buoyancy and a magnetically driven secondary instability. This mechanism arises naturally out of the dynamics of the system and provides, to the best of our knowledge, the first

example of a fully self-consistent dynamo in which magnetic buoyancy is crucial to the generation process. A remarkable property of this system is that the regeneration of poloidal field can be interpreted as an α-effect even though there is no rotation and hence no Coriolis force present.

2. FORMULATION

We study the evolution of magnetic fields in a stably stratified, fully compressible atmosphere with an imposed forcing to drive a parallel shear flow. We consider a perfect gas in a Cartesian domain with aspect ratio $x_m : y_m : 1$, with z increasing downward, and of vertical depth d. In this geometry, we consider the x-direction to be toroidal and the y- and z-directions to be poloidal. The atmosphere is initially threaded by a horizontal poloidal magnetic field of strength B_0 and begins in hydrostatic equilibrium, so the temperature $T(z)$ and density $\rho(z)$ satisfy the polytropic relation

$$T(z) = T_0(1 + \theta z/d) \ , \tag{1}$$

$$\rho(z) = \rho_0(1 + \theta z/d)^m \ . \tag{2}$$

Here T_0 and ρ_0 are the temperature and density at $z = 0$, θ is the temperature contrast, and m is the polytropic index.

We assume that the specific heats c_p and c_v, dynamic viscosity μ, thermal conductivity K, magnetic diffusivity η, and gravitational acceleration are constant. We non dimensionalize the equations by adopting T_0, ρ_0, and B_0 as the units of temperature, density, and magnetic intensity, the depth of the layer d as the unit of length, and the isothermal sound crossing time $d/[(c_p - c_v)T_0]^{1/2}$ as the unit of time. The evolution equations for the velocity $\boldsymbol{u} = (u, v, w)$, magnetic field $\boldsymbol{B} = (B_x, B_y, B_z)$, density ρ, temperature T, and pressure p thus become

$$\partial_t \rho + \boldsymbol{\nabla} \cdot (\rho \boldsymbol{u}) = 0 \ , \tag{3}$$

$$\partial_t(\rho \boldsymbol{u}) + \boldsymbol{\nabla} \cdot (\rho \boldsymbol{u}\boldsymbol{u} - a_m \boldsymbol{B}\boldsymbol{B}) = -\boldsymbol{\nabla}\hat{p} + \rho\theta(m+1)\hat{z} + \mathrm{Pr}C_k\left[\nabla^2 \boldsymbol{u} + \tfrac{1}{3}\boldsymbol{\nabla}(\boldsymbol{\nabla} \cdot \boldsymbol{u})\right] + \boldsymbol{F} \ , \tag{4}$$

$$\partial_t T + \boldsymbol{\nabla} \cdot (\boldsymbol{u}T) + (\gamma - 2)T\boldsymbol{\nabla} \cdot \boldsymbol{u} = \gamma C_k \rho^{-1} \nabla^2 T + \zeta C_k a_m (\gamma - 1)\rho^{-1}|\boldsymbol{\nabla} \times \boldsymbol{B}|^2 + V_\mu \ , \tag{5}$$

$$\partial_t \boldsymbol{B} + \boldsymbol{u} \cdot \boldsymbol{\nabla}\boldsymbol{B} = \boldsymbol{B} \cdot \boldsymbol{\nabla}\boldsymbol{u} - \boldsymbol{B}\boldsymbol{\nabla} \cdot \boldsymbol{u} + \zeta C_k \nabla^2 \boldsymbol{B} \ , \tag{6}$$

$$\boldsymbol{\nabla} \cdot \boldsymbol{B} = 0 \ , \tag{7}$$

$$p = \rho T \ . \tag{8}$$

Here $\boldsymbol{F}$ is a forcing function;

$$C_k = K/\{d\rho_0 c_p[(c_p - c_v)T_0]^{1/2}\}$$

is the thermal dissipation parameter; $\mathrm{Pr} = \mu c_p/K$ is the Prandtl number; $\zeta = \eta c_p \rho_0/K$ is the magnetic Prandtl number; V_μ is the viscous heating; $\gamma = c_p/c_v$ is the ratio of specific heats; $Q = B_0^2 d^2/(\mu_0 \mu \eta)$ is the Chandrasekhar number, where μ_0 is the magnetic permeability; and $\hat{p} = p + a_m \boldsymbol{B}^2/2$ is the total pressure, with $a_m \equiv \mathrm{Pr}\zeta Q C_k^2$.

At the upper and lower boundaries, we impose stress-free, impenetrable velocity conditions and require that the vertical gradient of the horizontal components of the magnetic field vanish. This ensures that no magnetic flux will be transported through these boundaries, by either advection or resistive diffusion, so that the boundaries can play no role in maintaining magnetic fields within the domain. We impose a constant temperature on the upper surface and a fixed heat flux through the lower one so that

$$\partial_z u = \partial_z v = w = \partial_z B_x = \partial_z B_y = 0 \quad \text{at} \quad z = 0, 1 \ ; \tag{9}$$

$$T = 1 \quad \text{at} \quad z = 0 \ ; \quad \partial_z T = \theta \quad \text{at} \quad z = 1 \ . \tag{10}$$

We assume periodic boundary conditions in the horizontal directions.

The forcing function $\boldsymbol{F}$ in equation (4) is chosen to maintain a steady, stable target velocity profile $\boldsymbol{U}_0$ against

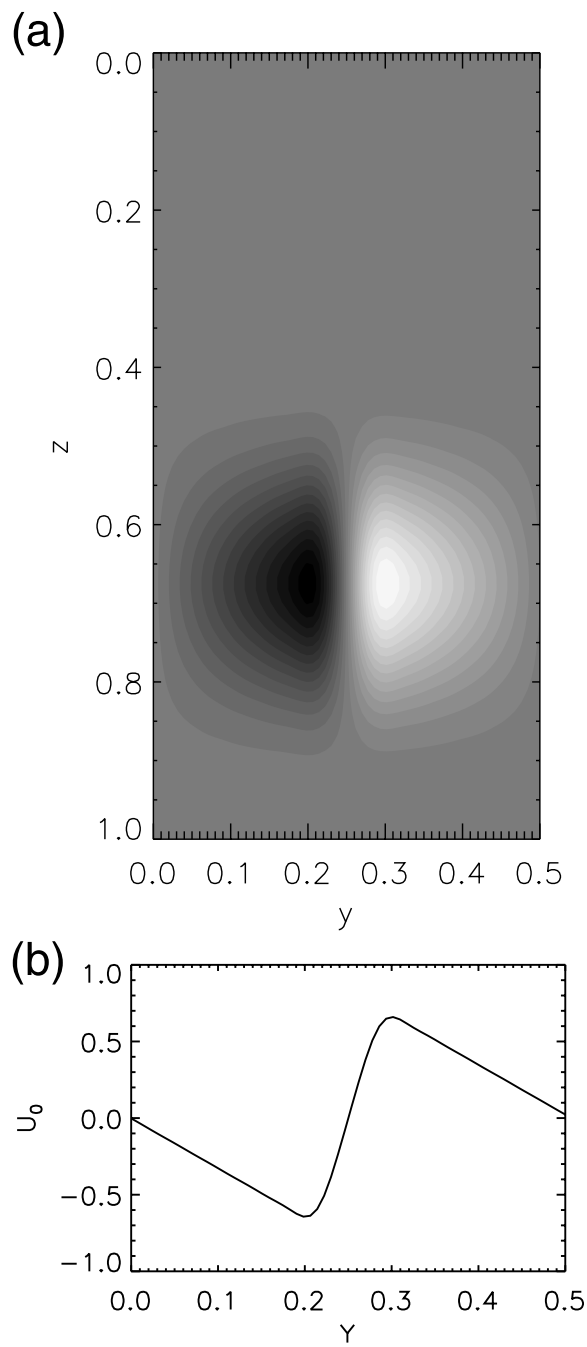

FIG. 1.—Target shear velocity profile $U_0(y, z)$ that defines the forcing $\boldsymbol{F}$. (*a*) Dark shades represent the flow u in the negative x-direction, and light shades represent flow in the positive x-direction. (*b*) Profile plotted vs. y at the depth of maximum forcing $z_v = 0.675$.

TABLE 1

PARAMETER VALUES FOR SIMULATIONS

Case	a_m	Re_m	$M_\mathrm{A}(t=0)$	Comment
A1	4.72×10^{-8}	955	5289	Decaying equilibrium
A2	4.72×10^{-7}	955	1673	Intermittent K-H dynamo
A3	4.72×10^{-6}	955	52.9	Intermittent K-H dynamo (different initial conditions)
A4	4.72×10^{-5}	955	167	Intermittent K-H dynamo (different initial conditions)
A5	4.72×10^{-4}	955	529	Intermittent K-H dynamo (different initial conditions)
M1	4.72×10^{-7}	477	1673	Intermittent K-H dynamo
M2	4.72×10^{-7}	1909	1673	No dynamo
M3	4.72×10^{-7}	3820	1673	Chaotic intermittent K-H dynamo
M4	4.72×10^{-7}	7639	1673	Chaotic intermittent K-H dynamo
M5	4.72×10^{-7}	15277	1673	Chaotic intermittent K-H dynamo
M6	4.72×10^{-4}	239	52.9	Nonintermittent, in-place K-H dynamo

NOTES.—Re_m and $M_\mathrm{A}(t=0)$ are here evaluated in terms of the initial polytropic state and the imposed values at $z=z_v$. In all cases, $\gamma=5/3$, $m=1.6$, $\theta=2$, $x_m=y_m=0.5$, $\mathrm{Pr}=0.016$, $C_k=0.3456$, $\mathrm{Ra}=-10^3$, and $U_f=0.66$. Note that Re_m is then set by ζ, and a_m merely establishes the intensity of the initial magnetic field imposed, $B_y^2(t=0)$.

viscosity, *in the absence of magnetic effects*. We choose the velocity to be in the x-direction and to be confined in the vertical to a layer between $z_0=0.4$ and $z_1=0.95$, with the strongest forcing halfway between these depths at $z_v=0.675$ (Fig. 1*a*). In the y-direction, the forcing function has a "sawtooth" profile (Fig. 1*b*). We note that this forcing is different from that in CBC, where the shear was a cosine function of y. The aim here is to produce a single magnetic structure rather than an interacting pair.

The functional form for $\boldsymbol{U}_0$ is given by

$$\boldsymbol{U}_0=(U_0,0,0)\ ,\quad U_0=U_f g(y)f(z)\ , \tag{11}$$

where U_f is the scalar amplitude of the forcing, $g(y)$ describes the sawtooth profile, and $f(z)$ is the quartic polynomial that matches smoothly to zero at z_0 and z_1. Because the nonlinear advective term in equation (4) for this velocity is identically zero, setting $\boldsymbol{F}=(F,0,0)$ with $F=-\mathrm{Pr}C_k\nabla^2U_0$ with no magnetic field present will force the initial condition $\boldsymbol{u}=0$ to evolve to $\boldsymbol{U}_0$.

The magnetic initial conditions are chosen so that the system contains no net flux; thus, in the absence of any flow, the magnetic field will resistively decay to zero. Specifically, $\boldsymbol{B}=(0,B_y(z),0)$, initially, with

$$B_y(z)=\begin{cases}+1\ , & z>\frac{1}{2}\ ,\\ -1\ , & z<\frac{1}{2}\ .\end{cases} \tag{12}$$

This should be contrasted with CBC, where $B_y=+1$ everywhere, so that the system contained a net flux.

The stability of the atmosphere to (nondissipative) convective motions is measured by the subadiabatic gradient

$$\nabla-\nabla_\mathrm{ad}=\theta\left[1-\frac{(m+1)(\gamma-1)}{\gamma}\right]\ . \tag{13}$$

Throughout this paper, we choose $\theta=2$, $\gamma=5/3$, and $m=1.6$ so that $\nabla-\nabla_\mathrm{ad}=-0.08$ (i.e., the layer is convectively stable). For a fluid with finite viscosity and thermal conductivity, a more precise measure of stability to convection is the Rayleigh number

$$\mathrm{Ra}\equiv\frac{\theta^2(m+1)}{\sigma C_k^2}\left[1-\frac{(m+1)(\gamma-1)}{\gamma}\right](1+\theta z)^{2m-1}\ , \tag{14}$$

which we quote at middepth for each case in Table 1. The intensity of the initial magnetic field is given by the Chandrasekhar number Q. It should be noticed that the choice of nondimensionalization using B_0 that leads to the appearance of Q as a parameter is not ideal for this problem. It has been adopted here for continuity with the work in CBC. However, there is an important difference between this work and the former. In CBC, there is an initial net horizontal magnetic flux that is necessarily maintained for all time, and therefore it can be used to construct a meaningful unit of magnetic field intensity. Here the net flux is zero, and the problem is to ascertain whether magnetic field either decays or grows through a dynamo process. Therefore, there is no clear *characteristic* magnetic field strength, and Q defines only the *initial* field intensity. A more meaningful nondimensionalization of the magnetic field strength would be in terms of the units of the fluid velocities, and indeed, this is what is generally done in dynamo problems as opposed to magnetoconvection problems.

The choice to continue the parameterization of CBC here allows comparison with the previous work but essentially leaves Q as a parameter that dictates only the nature of the initial conditions. It is helpful then to evaluate the magnetic field strength in terms of its equivalent Alfvén speed relative to some characteristic velocity. To this end, we define

$$M_\mathrm{A}\equiv\frac{U_f}{B_y}\sqrt{\frac{\rho}{a_m}}\ , \tag{15}$$

which relates the Alfvén speed to the shear velocity.

To describe the importance of the viscous, magnetic, and thermal diffusivities relative to advection, we define the Reynolds number Re, magnetic Reynolds number Re_m, and the Peclet number Pe by

$$\mathrm{Re}\equiv\frac{U_f y_m\rho}{\sigma C_k}\ , \tag{16}$$

$$\mathrm{Re}_m\equiv\frac{U_f y_m}{\zeta C_k}\ , \tag{17}$$

$$\mathrm{Pe}\equiv\frac{U_f y_m\rho}{\gamma C_k}\ , \tag{18}$$

where ρ is measured (in the initial polytropic state) at the depth of maximum shear.

The evolution equations are solved numerically by using a hybrid pseudospectral/finite difference scheme with

spatial resolution of 64^3. For further details of the numerical methods see Tobias et al. (2001).

3. NUMERICAL SIMULATIONS

We have carried out a series of numerical simulations with the following parameters: $U_f = 0.66$, $\mathrm{Pr} = 0.016$, $C_k = 0.3456$, and $x_m = y_m = 0.5$. These correspond to a Reynolds number $\mathrm{Re} = 234$ and a Rayleigh number $\mathrm{Ra} = -10^3$. A preliminary simulation has confirmed that for this Reynolds number the system is hydrodynamically stable.

The magnetic evolution of the system was investigated by carrying out a series of simulations with varying strength of the initially imposed magnetic field, via a_m, and magnetic Reynolds number Re_m through ζ (see Table 1).

Many of the basic mechanisms and behaviors of this system are similar to those in CBC, including nonstatic equilibria at moderate magnetic Reynolds numbers, the regular production of rising magnetic structures at higher magnetic Reynolds numbers, and the ability of a magnetic buoyancy flow to trigger a three-dimensional Kelvin-Helmholtz instability, which displaces magnetic structures into a helical shape.

3.1. *Weak Initial Field: No Dynamo*

We first consider a case with weak initial magnetic field (case A1). At these parameters, the system evolves to a nonstatic (quasi) equilibrium in a similar manner to cases described in CBC. The shear flow, growing from rest toward the target velocity, creates strong toroidal magnetic field B_x with opposing signs in two regions, resembling the magnetic flux tubes of ideal MHD theory. This is shown in Figure 2 as a series of volume renderings of the computational domain at successive times. The forcing has caused the toroidal shear flow u to grow and quickly reach a steady state, as seen in Figure 3*a*.

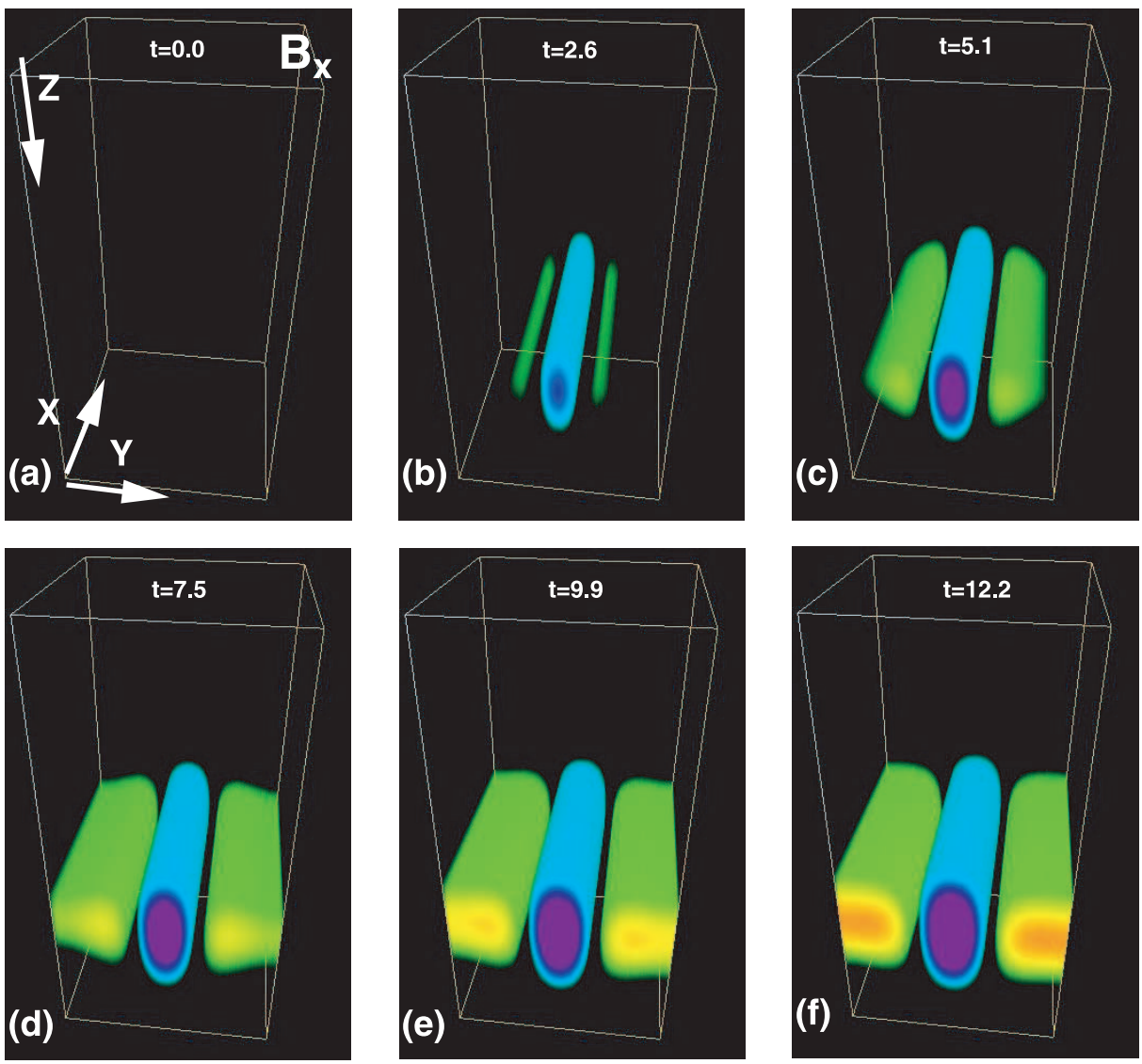

FIG. 2.—Creation of strong, tubelike magnetic structures by the velocity shear. Shown are volume renderings of toroidal magnetic field B_x. Here (and in subsequent volume renderings of this type) cool opaque colors (blue–green) represent negative toroidal field $B_x < 0$, and warm colors (red–yellow) represent positive toroidal field $B_x > 0$. The case A1 is shown from time $t = 0$ to 12.2, when two tubelike strong toroidal (x-directed) magnetic structures are formed over time by the action of the velocity shear on the initial weak poloidal (y-directed) magnetic field.

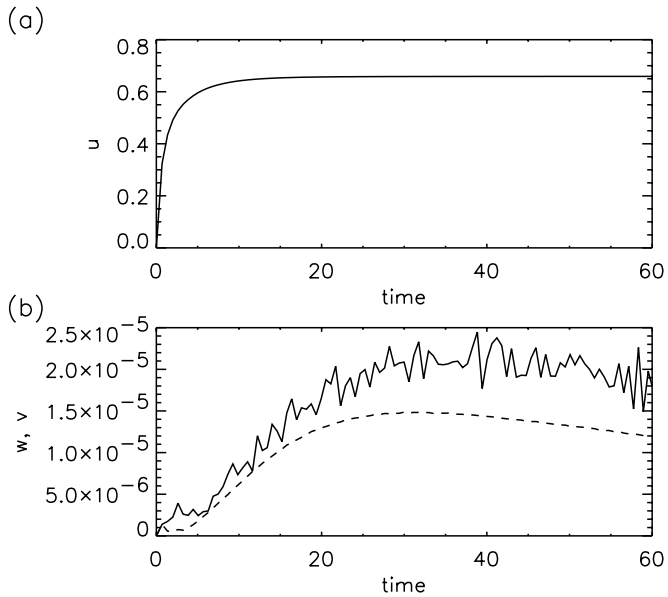

FIG. 3.—Build up of toroidal and poloidal velocities with time for case A1. (*a*) Maximum values of u and (*b*) maximum values of w (*solid line*) and v (*dashed line*) vs. time. All begin at zero, increase, and then saturate when the nonstatic (quasi) equilibrium state is reached. The noise in w is caused by vertical sound waves in the domain, a transient behavior.

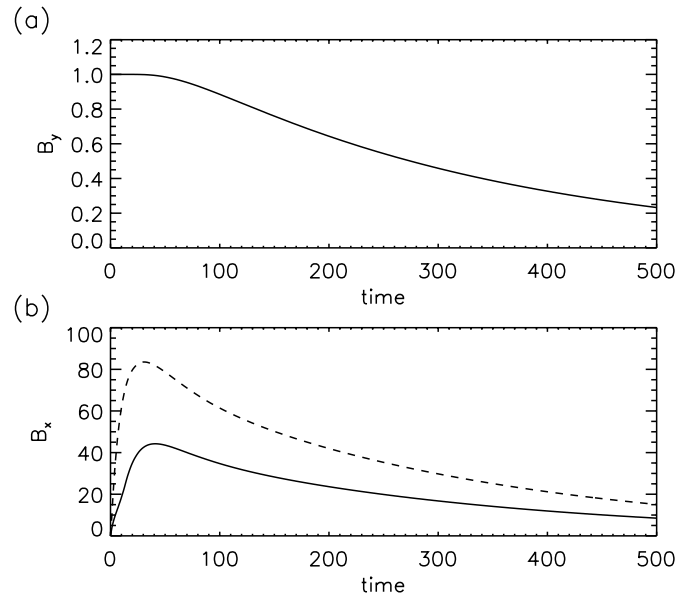

FIG. 5.—Decay of the magnetic fields in the (quasi) equilibrium for case A1. The maximum values of (*a*) the poloidal field component B_y and (*b*) the toroidal field B_x along with $|\min B_x|$ are shown vs. time. Although strong toroidal field is created, all magnetic fields eventually decay away since there is no dynamo action.

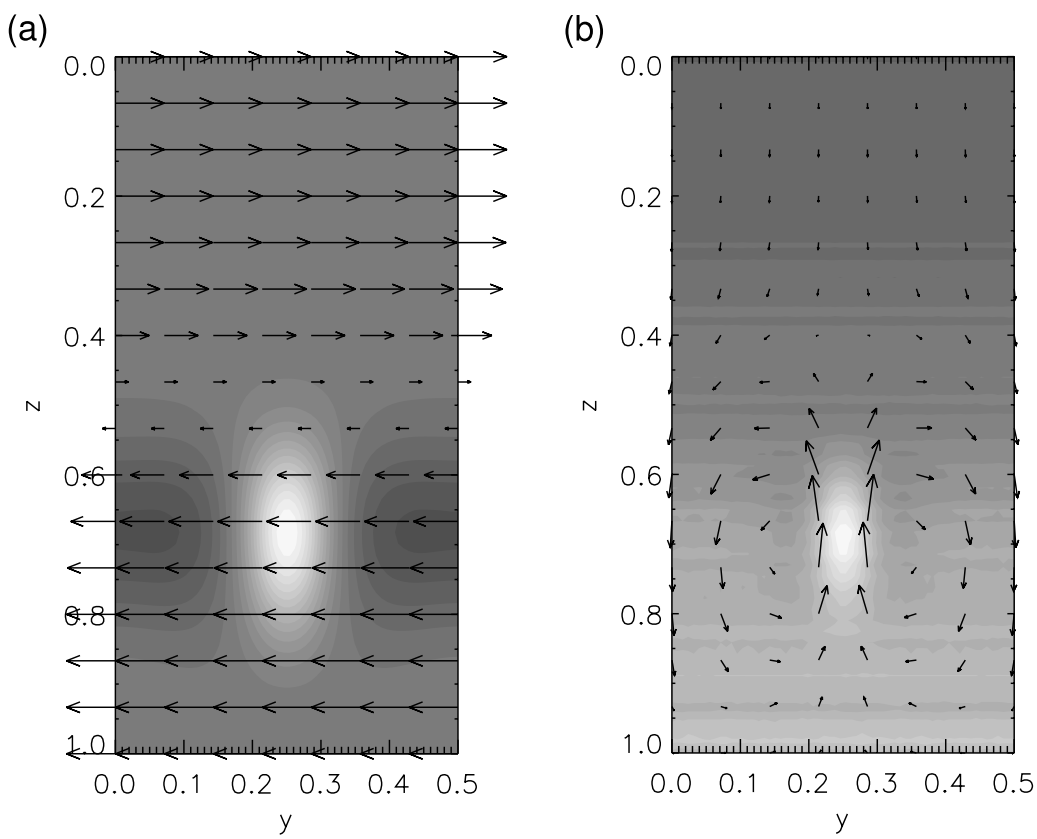

FIG. 4.—Dynamics associated with the nonstatic (quasi) equilibrium achieved in case A1 at $t = 12.2$. (*a*) Magnetic fields averaged over the x-direction; poloidal field (B_y, B_z) is indicated by arrows, and toroidal field (B_x) by shading (*dark*, positive; *light*, negative). (*b*) Poloidal flow (v, w) indicated by arrows, together with the density perturbation indicated by shading (*light*, density deficit; *dark*, density excess). This figure is a y-z cross section of the domain at arbitrary x (since the system is x-invariant).

Figure 4*a* shows the magnetic field components averaged in the x-direction. It shows that the poloidal field is still essentially the initial field, with $B_y = +1$ above $z = \frac{1}{2}$ and $B_y = -1$ below. Because the flow has both positive and negative shear $\partial_y u$, it generates a strong toroidal field with negative B_x near $y = 0.25$, surrounded by a weaker field with positive B_x. Magnetic pressure causes the magnetized regions to expand in order to maintain total pressure equilibrium with a corresponding decrease in density (Fig. 4*b*). The resulting horizontal density gradients drive a poloidal flow resembling a convective roll, as shown by the arrows in Figure 4*b*. Because magnetic forces are weak, the flow velocities are correspondingly small, as shown in Figure 3*b*. The noise that appears in w is the result of sound waves in the layer. The system quickly reaches a stable nonstatic equilibrium in which the production of field by induction in the shear layer is everywhere balanced by resistive diffusion and advection from the magnetic buoyancy–driven flow.

If the simulation is continued for a long time (500 sound crossing times), the poloidal field B_y eventually decays away, with the positive field ($z > \frac{1}{2}$) canceling out the negative field ($z < \frac{1}{2}$). Hence, this tube state is only a *quasi*-equilibrium unlike that actual equilibrium state found in CBC. An estimate of the e-folding time for this process can be computed to be approximately 300 from the time history of the maximum value of B_y (Fig. 5*a*).

3.2. *Stronger Initial Field: Kelvin-Helmholtz Instability*

If the intensity of the initial magnetic field is increased by a factor of $\sqrt{10}$ (a tenfold increase in a_m; case A2), the evolution proceeds initially in a similar manner to case A1, except that the poloidal flows are stronger (Fig. 7). At $t \approx 40$, a new behavior appears that breaks the translational symmetry in the x-direction and, as shown below, allows the generation of poloidal field and therefore the possibility of dynamo action. The central negative toroidal magnetic structure is twisted into two helical shapes, while a new positive toroidal magnetic structure appears between them,

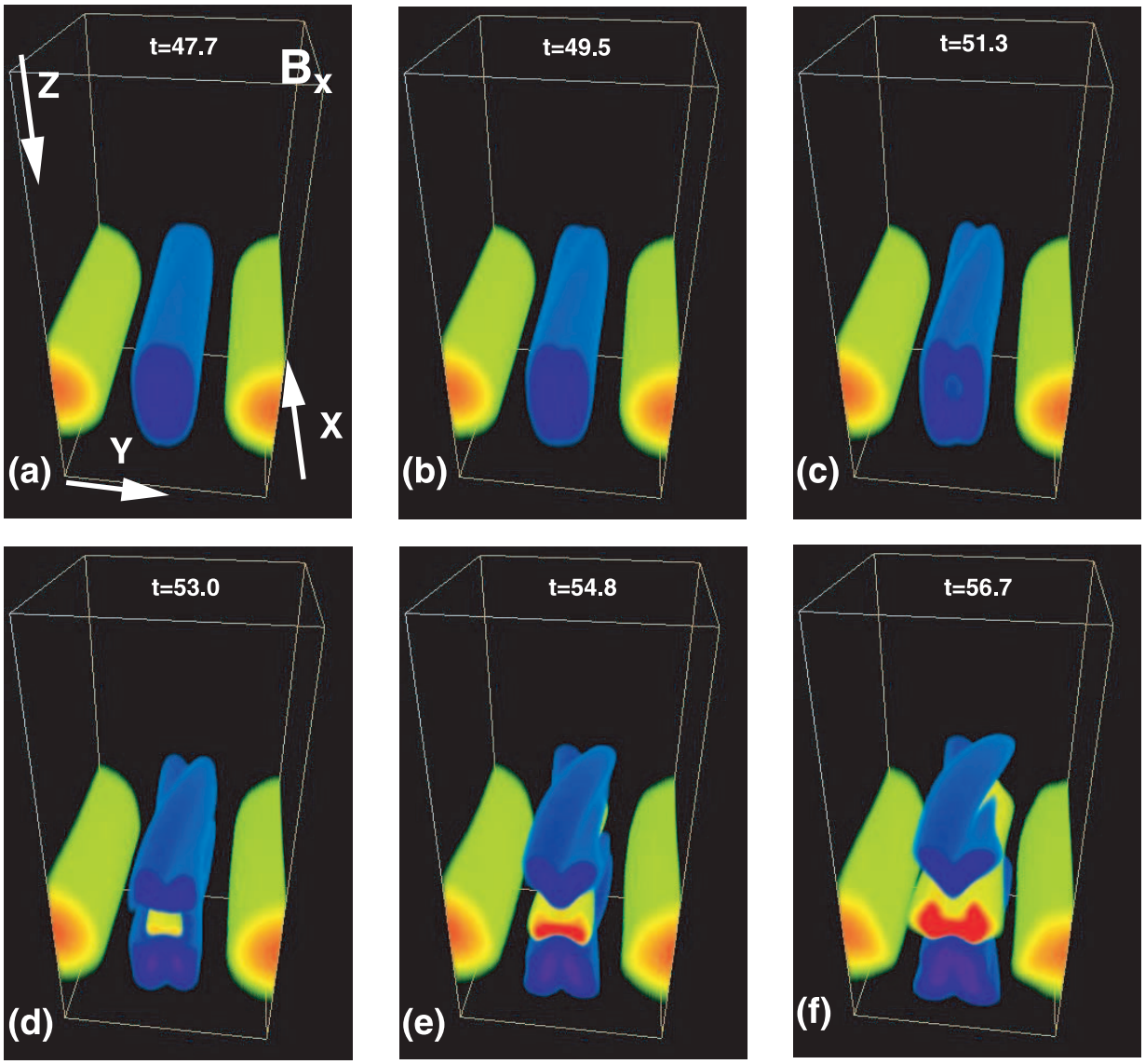

FIG. 6.—K-H instability breaks the x-invariance of the system, twisting the center toroidal structure into helical shapes. Volume renderings of B_x are shown from case A2 at times between $t = 47.7$ and 56.7.

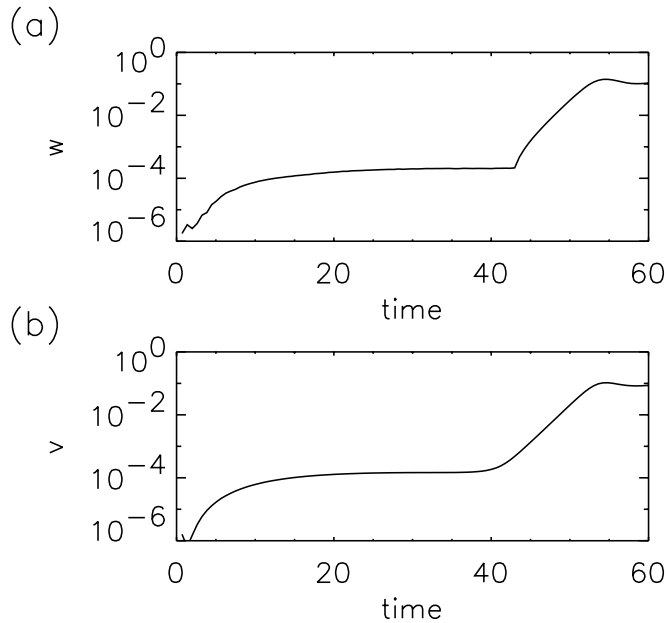

FIG. 7.—Onset of a K-H instability in case A2. Plotted are the maxima of the poloidal components of the flow, (*a*) w and (*b*) v against time. Magnetic buoyancy generates a steady roll-like poloidal flow initially, until $t \approx 40$. At that time, the solution becomes dominated by an exponential growth of the poloidal velocities (suggesting a linear instability) until saturation at $t \approx 55$.

leaving fragments of the negative structure above and below (Fig. 6).

The poloidal flow that twists the negative magnetic structure in this manner is the result of an instability, as revealed by the exponential growth of v and w that becomes apparent around $t \approx 40$ (Fig. 7). The nature of the instability can be understood by examining the horizontal flow field (u, v) at the depth of maximum forcing before and after the instability. At $t = 40$ (Fig. 8*a*), only the parallel shear flow u is apparent. By $t = 54.8$ (Fig. 8*b*), a significant flow v has appeared, with a form like $v \propto \sin x/x_m$, suggesting that the instability is of the Kelvin-Helmholtz (K-H) type (see, e.g., Drazin & Reid 1981).

The flow (u, w) likewise contains K-H modes in the vertical direction. Plotting (u, w) in the plane $y = 0.20$ (where u is originally a minimum) shows that two vertical modes have appeared between times $t = 40.0$ (Fig. 8*c*) and $t = 56.8$ (Fig. 8*d*); above $z = z_v$, $w \propto -\cos 2\pi x/x_m$, whereas below, $w \propto +\cos 2\pi x/x_m$. The same K-H modes also appear in the plane $y = 0.30$ where u is maximal. Because the Reynolds number is moderate, the K-H instability saturates fairly quickly (by $t \approx 55$) with poloidal velocities that are only about $\frac{1}{4}$ of the toroidal velocity.

The phase difference between the vertical and horizontal K-H modes causes the central magnetic structure to be displaced into the helical shape shown in Figure 6. This action tilts the field B_x into the y- and z-directions, thus creating field B_y and B_z in the form of a poloidal loop. To illustrate this, Figure 9 shows the components of the magnetic field averaged in the x-direction, with the poloidal field (B_y, B_z) indicated by vector arrows at various times. Before the K-H instability, at $t = 40.0$ (Fig. 9*a*), the remains of the initially imposed poloidal field $B_y(z)$ can be seen as it resistively diffuses. The shear flow u has stretched the $B_y(<0)$ field in the toroidal direction, creating a strong toroidal magnetic structure with $B_x < 0$, centered on $y = 0.25$, $z = 0.675$, and a weaker positive magnetic structure at $y = 0$, $z = 0.675$. As the K-H instability proceeds (Figs. 9*b* and 9*c*), the K-H modes twist the toroidal structure, creating two poloidal loops, centered at $y = 0.25$, $z \approx 0.65, 0.75$, above and below the center of the toroidal structure. Because the vertical w-modes of K-H instability reverse sign above and below the shear layer, they create opposing poloidal loops, so that above the layer ($z \approx 0.65$) it is counterclockwise with a negative x-component of $\nabla \times \boldsymbol{B}$ and below the layer ($z \approx 0.75$) it is clockwise with $\nabla \times \boldsymbol{B} \cdot \hat{x} > 0$ (note that z is downward). Together, these two poloidal loops both create a strong field $B_y > 0$ at the line of maximum shear $y = 0.25$, $z = z_v$. This field is then stretched out by the shear $\partial_y u < 0$, so that by $t = 52.4$ (Fig. 9*d*), it has created a new magnetic structure with positive toroidal field $B_x > 0$ (at $y = 0.25$, $z = 0.65$) because the source term $B_y \partial_y u$ is now positive at this location.

Following the onset of the K-H instability, a sequence of events can be discerned that can be considered a dynamo cycle:

1. The field is initially purely poloidal.
2. The poloidal field is sheared to create toroidal field.
3. The toroidal field induces a poloidal flow by magnetic buoyancy.
4. The poloidal flow steepens the shear and triggers a K-H instability.
5. The K-H modes twist the toroidal magnetic structure into a helical shape with a significant poloidal component.
6. The poloidal field is sheared to create new toroidal field.

Not only has this process demonstrated the regeneration of poloidal and toroidal magnetic fields, it has significantly amplified them. Since the toroidal field in the central magnetic structure ($B_x \approx -80$) is much stronger than the initial poloidal field when the K-H instability occurs, it quickly creates a very strong poloidal field (Fig. 10*a*), which in turn leads to the creation of even stronger toroidal field (Fig. 10*b*).

3.3. *A Series of Magnetic Structures*

The behavior of the system over a longer period of time can be seen from Figure 11, which shows the extreme values of B_x as a function of time. A number of interesting features are apparent from this figure. First, the system operates as a dynamo since the magnetic field does not appear to decay away. Second, strong toroidal field is generated in a cyclic manner. Third, the polarity of the strong toroidal field occasionally reverses. For instance, between $t = 70$ and 220, the system produces eight negative toroidal magnetic structures before reversing polarity after $t \approx 220$. Before examining the mechanism for polarity reversal, we wish to understand the mechanism that repeatedly produces magnetic structures of the same polarity.

Figures 12 and 13 show the evolution of the magnetic structure over one basic (nonreversing) cycle in volume renderings and in plots of the x-averaged magnetic field components. The corresponding changes in velocity are shown in Figure 14.

1. The system begins with a fairly well ordered poloidal field that is clockwise, i.e., $\nabla \times \boldsymbol{B} \cdot \hat{x} < 0$, and generally

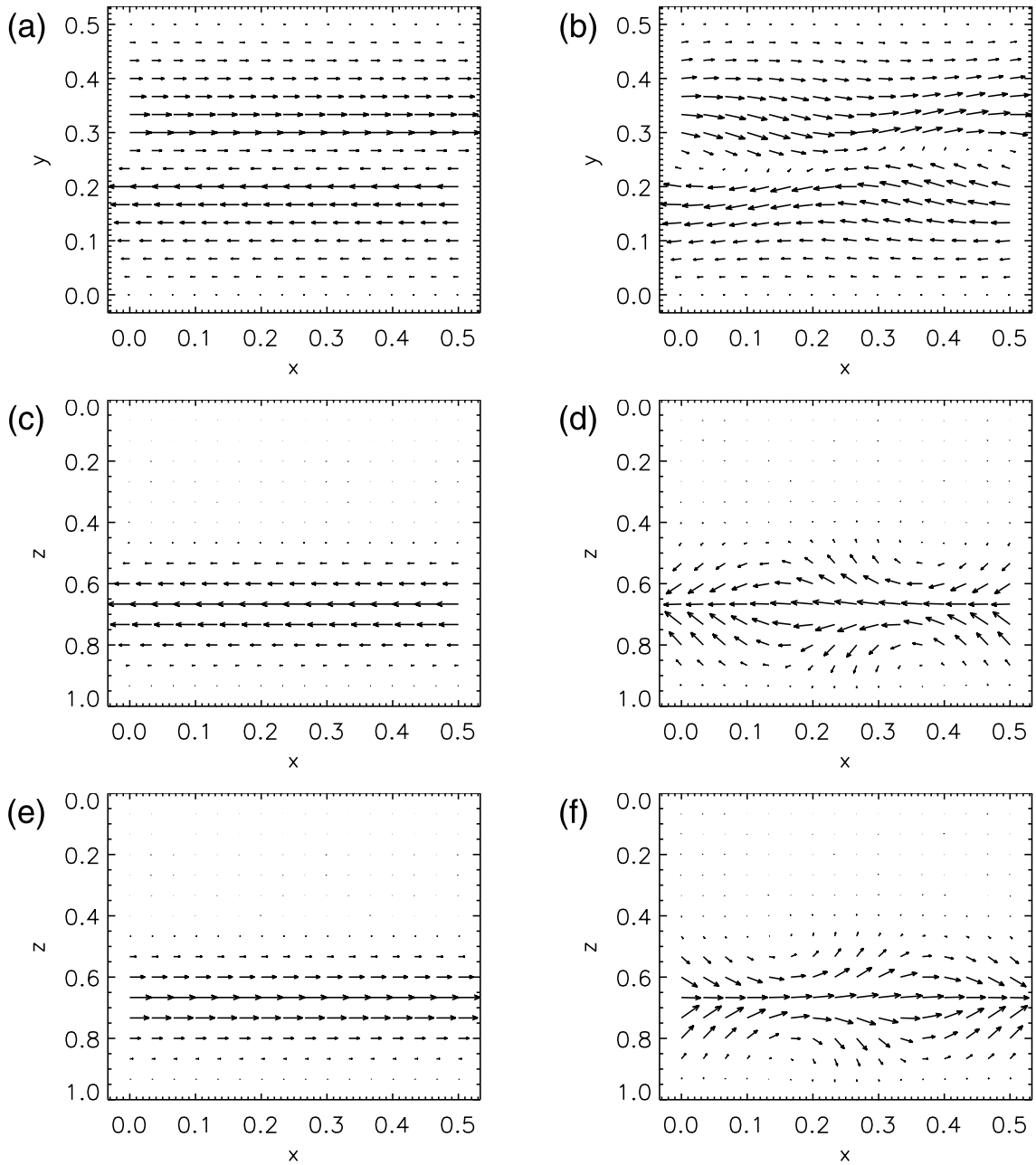

FIG. 8.—Morphology of the K-H instability. Plotted are flow fields from case A2 before the K-H instability at $t = 40$ (*left*) and during the instability at $t = 54.8$ (*right*). (*a*, *b*) Horizontal flow field (u, v) at depth $z = z_v$; (*c*, *d*) (u, w) at $y = 0.20$; (*e*, *f*) (u, w) at $y = 0.30$. In these plots, the amplitude of u has been reduced by a factor of 5 for clarity.

$B_y > 0$ in the upper half of the domain and $B_y < 0$ in the lower half (Fig. 13*a*). This field has produced a strong negative toroidal structure at $z \approx z_v$.

2. Over the next ≈8 sound crossing times (Figs. 13*b* and 13*c*) the poloidal field bends around the structure as it rises upward and diffuses. This spreads negative toroidal field throughout the central shear region.

3. The flow created by the rising structure triggers a K-H instability, characterized by a sharp rise in v and w and the drop in u. The instability acts on the toroidal magnetic field to produce two opposing poloidal loops (Figs. 13*d* and 13*e*). The lower poloidal loop is clockwise ($\nabla \times \boldsymbol{B} \cdot \hat{x} < 0$) and thus complementary to the poloidal field of Figure 13*a*, while the upper loop is counterclockwise ($\nabla \times \boldsymbol{B} \cdot \hat{x} > 0$), opposing the previous poloidal field.

4. Together, these two loops reverse the sign of B_y in the central shear region. The shear then stretches this to create positive toroidal field, with approximately 30% the intensity of the negative toroidal field from step 1.

5. This positive toroidal field rises slightly and, caught by the remaining K-H modes, creates a clockwise poloidal loop ($\nabla \times \boldsymbol{B} \cdot \hat{x} < 0$) in the upper region (Figs. 13*f* and 13*g*). Note that the K-H modes near $z \approx 0.5$ produce a counterclockwise poloidal loop in Figure 13*d* and a clockwise loop in Figure 13*f* because the toroidal field in this region has reversed sign (from negative to positive).

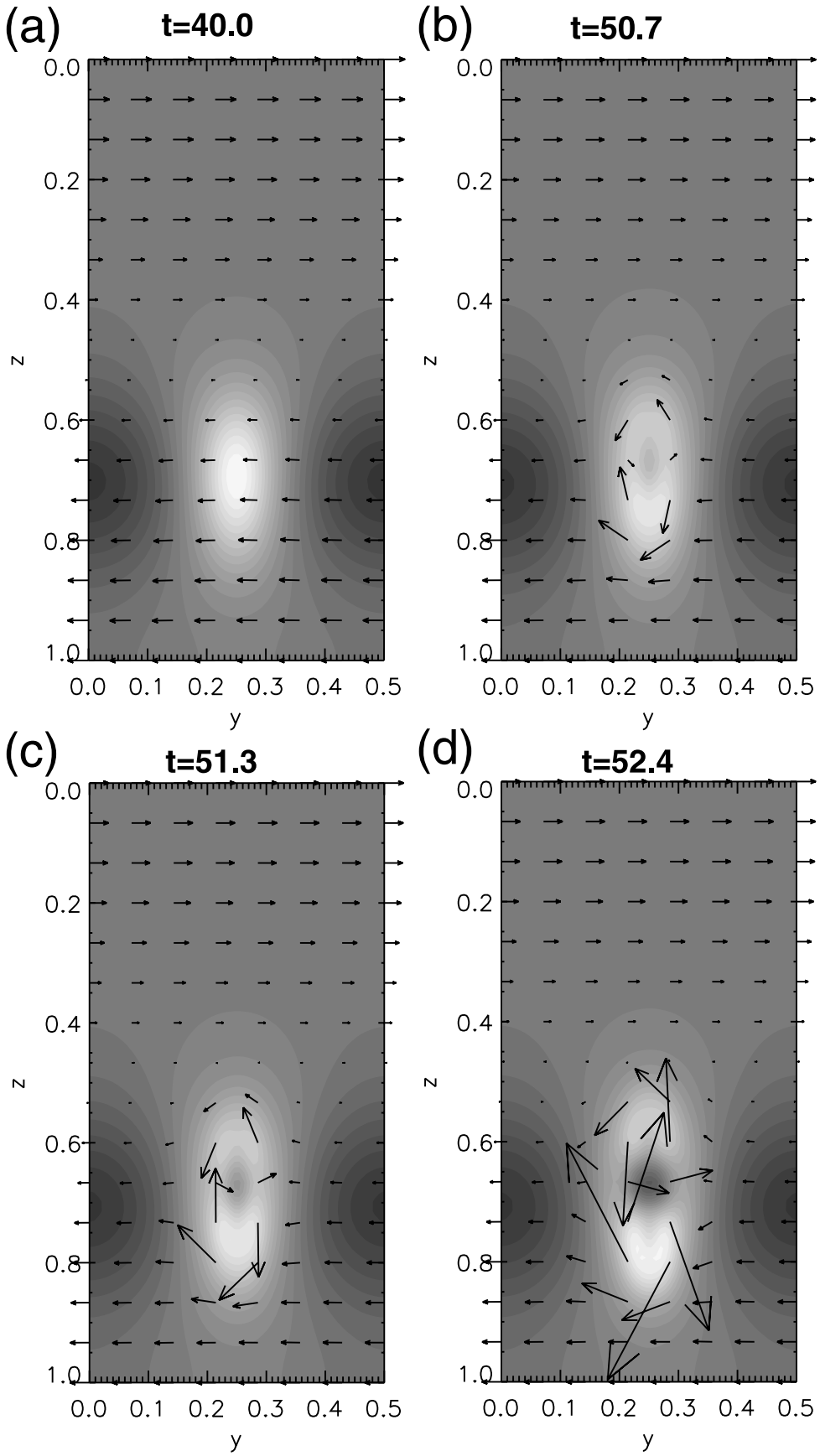

FIG. 9.—Creation of poloidal magnetic field via the K-H instability in case A2. Shown are magnetic fields averaged across the x-direction, with poloidal field (B_y, B_z) indicated by arrows and toroidal field B_x shaded (*dark*, positive; *light*, negative), for times $t = 40.0$–52.4. The toroidal field is twisted into helical shapes, thus creating two opposing poloidal loops centered around $y = 0.25$, $z = 0.65, 0.75$.

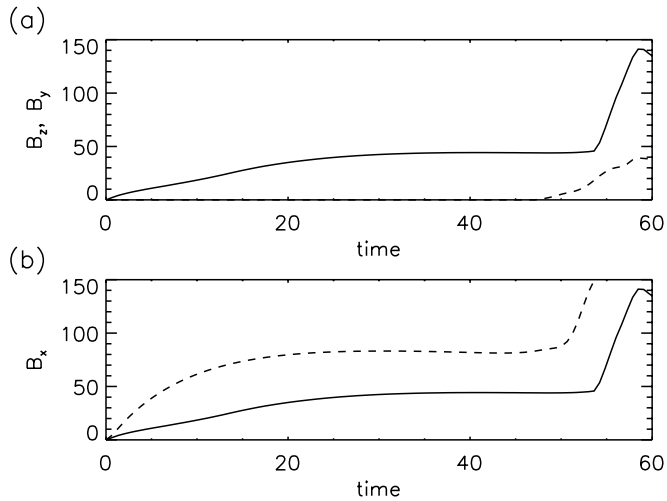

FIG. 10.—Strong poloidal and toroidal field are created in the dynamo cycle. Plotted are the maximum values of (*a*) B_z (*solid line*) and B_y (*dashed line*) and (*b*) B_x (*solid line*), together with $|\min B_x|$ (*dashed line*), vs. time for case A2. The newly created loops for $t > 50$ have a much stronger poloidal field than the system began with, thus causing the creation of even stronger toroidal field.

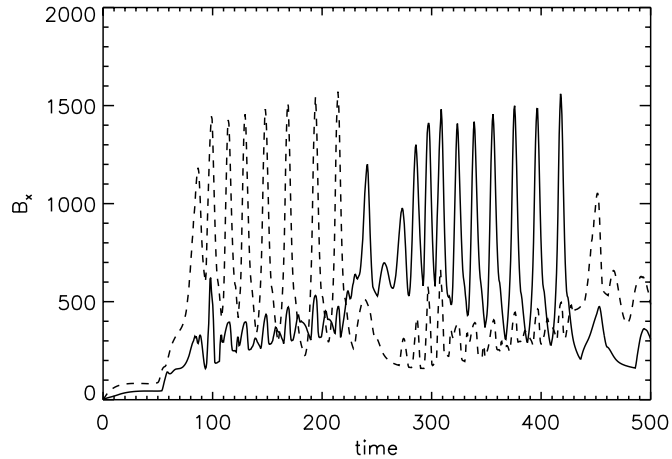

FIG. 11.—Longer time evolution of the system observed in toroidal magnetic field for case A2, exhibiting toroidal structure production with a change of polarity. Shown are the maximum values of B_x (*solid line*) and $|\min B_x|$ (*dashed line*) vs. time. Each toroidal structure creates a sharp peak in the minimum toroidal field, so the system produces eight negative toroidal structures between $t = 80$ and 220. Subsequently, the system changes polarity at $\approx$220 and produces about nine positive toroidal structures between $t = 250$ and 430.

6. After some resistive diffusion, the two clockwise poloidal loops (at $z \approx 0.5$ and $z \approx 0.7$) combine with the rest of the poloidal field in the domain, and the system builds another strong negative magnetic structure in the central shear region, so Figure 13*h* is almost identical to Figure 13*a*.

After the system produces about eight negative toroidal structures, at $t \approx 220$ the magnetic fields in the system *reverse polarity*, and the system then produces a series of rising magnetic structures with positive toroidal field (Fig. 11). To understand why the poloidal and toroidal fields of the system reverse polarity, first note that in Figure 11 the final negative toroidal magnetic structure was the most intense one produced until that time. Considering the x-averaged fields in Figure 15, one can see that the system at $t = 220$ contains a negative clockwise poloidal field ($\nabla \times \boldsymbol{B} \cdot \hat{x} < 0$) and produces a very strong negative toroidal structure (Fig. 15*a*). This structure rises, and the poloidal field lines bend around it, as before (Figs. 15*a*–15*c*). However, this time the rising of this stronger magnetic structure advects much of the shear layer with it, "dragging in" positive toroidal field (from $y = 0$) horizontally into the central shear region (at $y = 0.25$). Figure 15*d* does not show two opposing poloidal loops, above and below the central shear region, both made from the same toroidal field (Fig. 13*e*). Instead, it shows a very dominant counterclockwise upper poloidal loop ($\nabla \times \boldsymbol{B} \cdot \hat{x} > 0$). The lower poloidal loop does not appear because strong negative toroidal field has been removed from this region. As more positive toroidal field is advected into the region (Figs. 15*e* and 15*f*), it creates a counterclockwise lower poloidal loop. By Figure 15*g*, both upper and lower poloidal loops are counterclockwise because they are created from opposing toroidal fields (whereas before they were created from the same toroidal field). In Figure 15*h*, these two loops have overcome the original poloidal field, leading to the creation of a positive toroidal structure in the shear layer, allowing the dynamo cycle to begin again but with reversed polarity.

After the polarity reversal, the system produces a series of magnetic structures in a process precisely opposite to what we saw in Figure 13, with a positive toroidal structure rising, triggering a K-H instability, creating opposing poloidal loops, and building another positive toroidal structure. This continues until it creates a structure strong enough to disrupt the shear layer again and reverse the polarity back again.

The possibility of polarity reversals gives rise to another interesting phenomenon that manifests itself in very long time integrations. One such integration is shown in Figure 16*a*, where the field evolution is followed over 2500 time units (eight resistive *e*-folding times). At certain epochs, the dynamo enters into episodes of reduced activity. Three such episodes are shown in Figure 16*b*, where the toroidal magnetic field drops to small values over several dynamo "cycles." During these intervals, magnetic fields appear to be resistively decaying, and there is no evidence of the K-H instability, as indicated by very weak values of the poloidal flow (Fig. 16*d*).

If we consider the x-averaged magnetic fields (Fig. 17), these events appear to be the result of a "failed" polarity reversal. A strong positive toroidal structure rises and advects negative toroidal field into the shear layer (Fig. 17*a*). The resulting poloidal loops (Fig. 17*b*) produce a negative toroidal structure in the shear layer (Fig. 17*c*), but it is weak, with a strength of $B_x \approx -25$ rather than the full amplitude of $|B_x| \approx 50$. This weak structure does not appear to rise, trigger the K-H instability, or generate poloidal loops (Figs. 17*d*–17*f*). Instead, the poloidal fields resistively diffuse, gradually getting weaker (Figs. 17*e*–17*g*), until a positive toroidal structure can be built that is strong enough to rise and trigger the K-H instability again, restarting the dynamo (Fig. 17*h*).

We established above (§ 3.1) that if the initial magnetic field is not strong enough, the flow induced by magnetic buoyancy is not strong enough to trigger the K-H instability (case A1). Therefore, there is a danger that if the magnetic fields in this system ever drop below that minimum value,

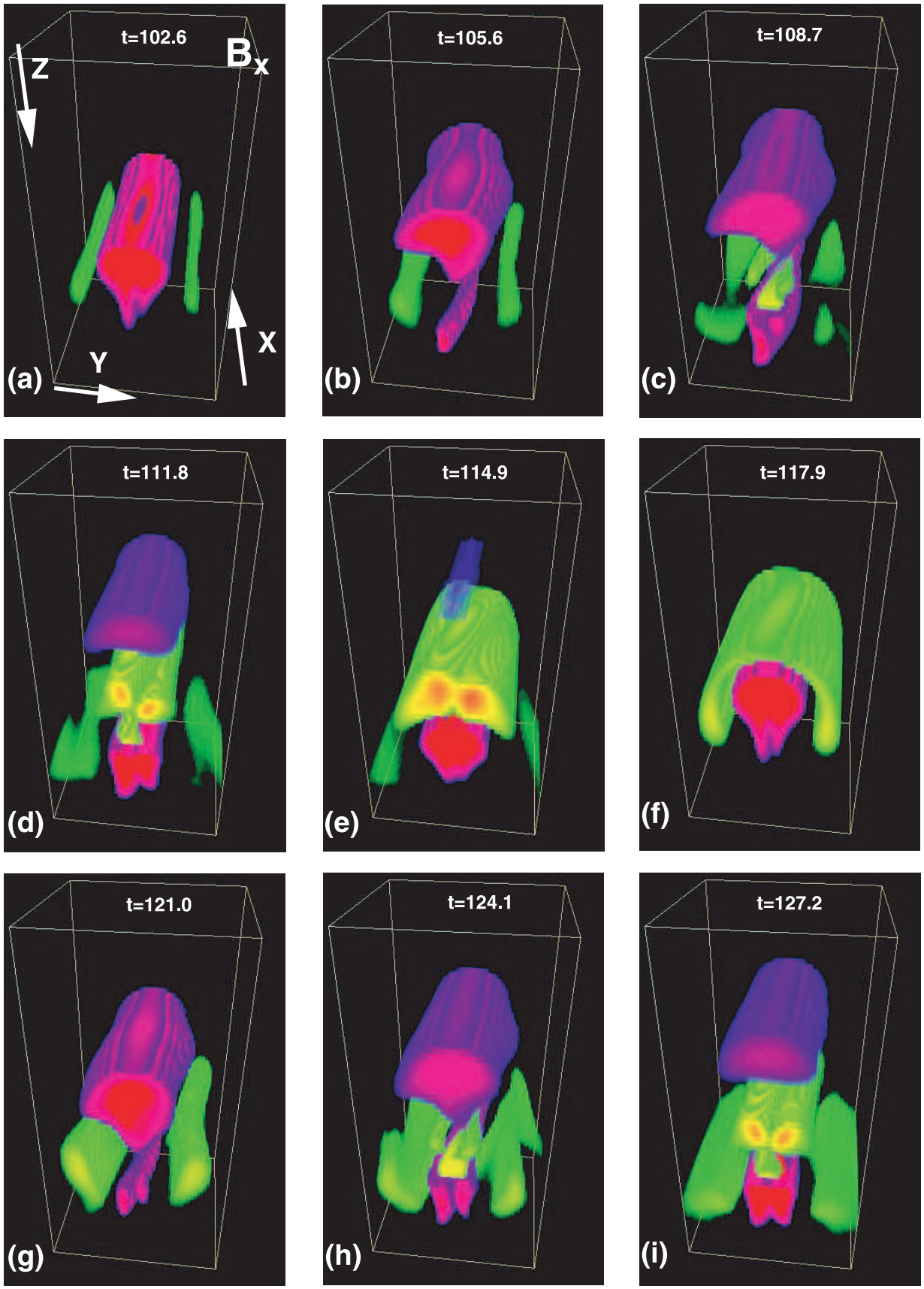

FIG. 12.—Production of a series of negative toroidal magnetic structures that each successively rise out of the shear layer. Volume renderings of B_x are shown from case A2 for times between $t = 102.6$ and 127.2 showing two such consecutive instances.

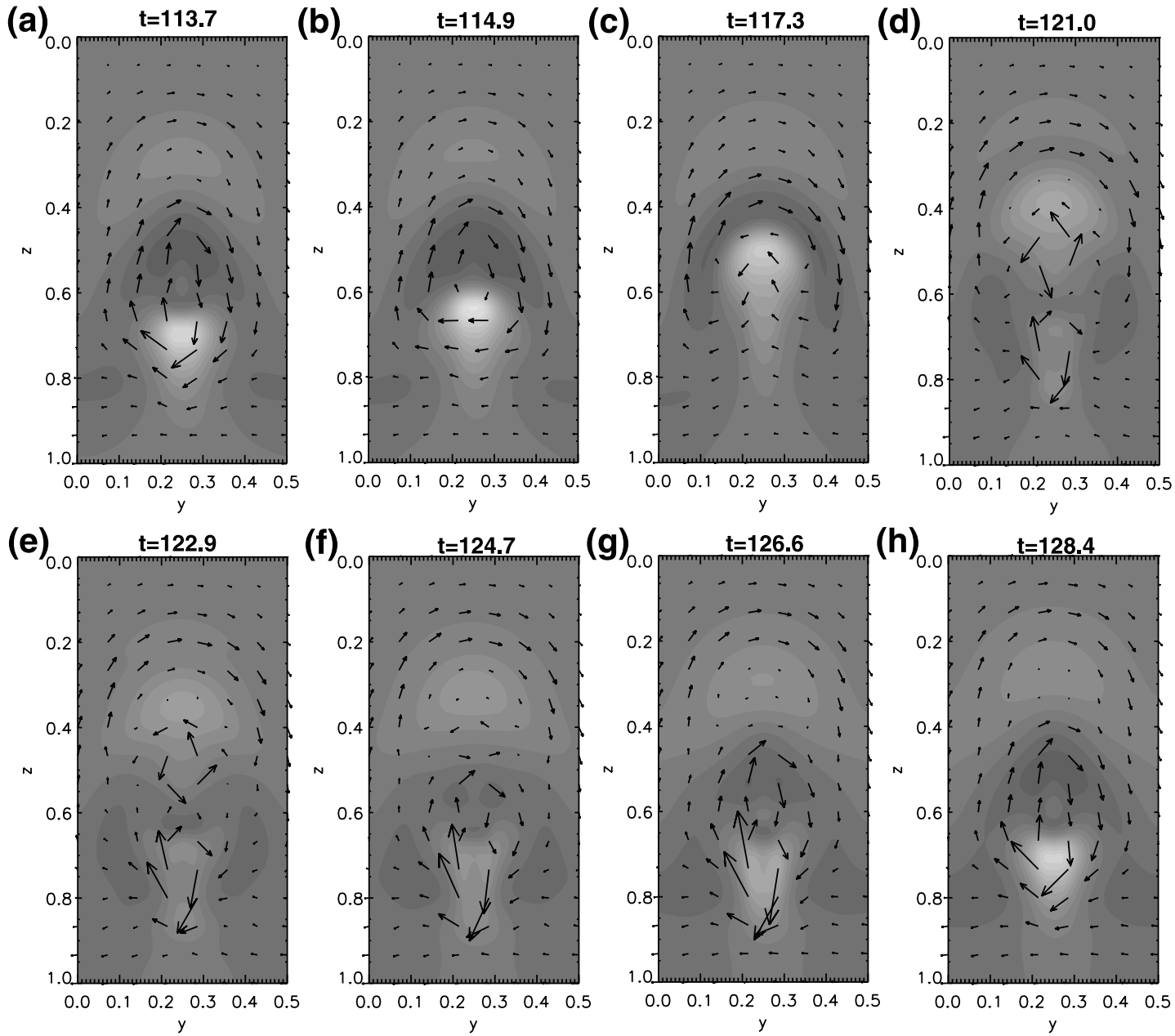

FIG. 13.—Dynamics of a full magnetic structure production cycle. Shown are the magnetic field averaged across the x-direction, with poloidal field (B_y, B_z) indicated with arrows and toroidal field B_y with shading (*dark*, positive; *light*, negative) from case A2, for $t = 113.4$ to 128.4. Initially, (*a*) the poloidal field is clockwise, and a negative toroidal structure is produced and rises (*a*–*c*). The action of rising triggers a K-H instability that creates two opposing poloidal loops, clockwise below $z = z_v$, counterclockwise above (*d*, *e*). These loops are sheared out to create positive toroidal flux, which is twisted into another clockwise poloidal loop (*f*, *g*). The K-H modes dissipate, and the clockwise loops diffuse throughout the domain, reestablishing the initial conditions (*h*).

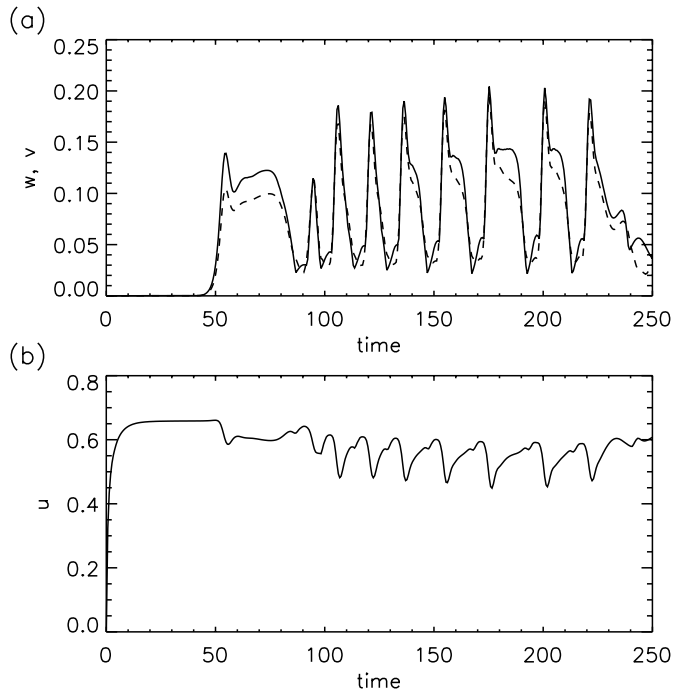

FIG. 14.—Long-time evolution of the system observed in velocity for case A2, exhibiting K-H instability. Shown are the maximum values of the velocities vs. time. The initial linear growth of the K-H instability (at $t \approx 50$) saturates before the toroidal flow has been significantly eroded. After this, a series of sharp peaks is seen in (*a*) the poloidal flow (v, w), accompanied by (*b*) drops in the toroidal flow, u, each indicating a K-H instability.

then it will permanently cease to be a dynamo. However, the saturation magnetic amplitude is approximately 10^3 times larger than the minimum field required to trigger dynamo action (as we saw in Fig. 11). Thus, it would take approximately $-\ln 10^{-3} \approx 6.9$ resistive timescales, which is $\approx$2000 sound crossing times, to resistively decay away below the threshold. The timescale necessary to build a toroidal field strong enough to trigger the K-H instability is thus the limiting factor to these three intervals. The forced horizontal shear has an amplitude of $\partial_y u \approx 10$, and thus it takes only $\approx$1 sound crossing time for this shear to amplify magnetic fields by a factor of 10 (neglecting magnetic diffusion). Because the resistive timescale is so much longer than this amplification timescale and because the minimum threshold for dynamo action is so much smaller than the saturation amplitude of the dynamo, it appears unlikely that dynamo action will ever completely cease, even though dynamo activity is somewhat irregular.

Since there is a lower threshold on the initial magnetic field to trigger dynamo action, it is natural to enquire as to whether higher values of the intensity of the initial field B_y lead to any different behavior in the system. Cases A3, A4, and A5 (see Table 1) were computed adopting simply higher values of the initial field. Each case, despite the different initial conditions and therefore the different approach to saturation, equilibrates to a state that is statistically the same as the other dynamo state (case A2) found. Although the saturated values of the magnetic field *appear* to be different, this is an artifact of the scaling adopted here [measuring in units of $B_y(t = 0)$ that change between cases], and in fact, each solution is merely a rescaling of the others (barring statistical differences). This is easily verified by measuring M_A by using the maximum norm of B_y in the dynamo phase as the measure in equation (15) (rather than the initial field used for the values in Table 1). Evaluating this shows that $M \approx 1$ for all the cases A2–A5 and that the dynamo saturates in equipartition with the shear energy source for these parameters.

3.4. *Effects of Varying* Re_m

To examine the effects of magnetic diffusion on this system, we vary the magnetic Prandtl number ζ from the case A2. First, in case M1, we increase the diffusivity by a factor of 2, resulting in a magnetic Reynolds number of $\mathrm{Re}_m = 477$ (compared with $\mathrm{Re}_m = 955$ for case A2). The result of this strong diffusion is that the initial poloidal field is quickly eroded with an *e*-folding time of $\approx$150. The system does not have time to trigger the K-H instability and so fails to behave as a dynamo.

If we decrease the magnetic diffusion (relative to case A2), so that the magnetic Reynolds number rises to $\mathrm{Re}_m = 1909$ (case M2), then a different behavior is observed (Fig. 18*a*). Rather than producing a series of toroidal magnetic structures at fairly regular intervals punctuated by irregular polarity reversals, the dynamo behaves in a much more chaotic manner. Structures are no longer produced at regular intervals, and the polarity is no longer obvious. There is no clear division of the evolution into intervals dominated by one or the other polarity, and often very strong positive and negative toroidal field are produced simultaneously. Similar chaotic results are observed for even higher values of Re_m (Figs. 18*b*–18*d*), except that the peak toroidal amplitudes produced increase.

3.5. *A Dynamo without Rising Magnetic Structures*

We established above that when magnetic diffusion is strong enough and magnetic forces are weak, the K-H instability is never triggered and the system does not act as a dynamo (case M1; $\mathrm{Re}_m = 477$, $a_m = 4.72 \times 10^{-7}$). However, this does not preclude the possibility that dynamo action is possible at this or still lower magnetic Reynolds numbers if magnetic forces are strong enough that the initial magnetic buoyancy flow can trigger the first K-H instability.

To examine this possibility, we increase the magnetic Prandtl number ζ, choosing a strong magnetic diffusion so that $\mathrm{Re}_m = 239$, but also increase the initial field strength by setting $a_m = 4.72 \times 10^{-4}$ (case M6). The resulting system does indeed trigger the first K-H instability and acts as a dynamo but in a qualitatively different manner to that we have seen so far.

As shown in Figure 19, this dynamo does not produce buoyantly rising toroidal structures. Instead, a single toroidal structure remains in the shear layer, slowly spiraling around to maintain the poloidal field. Rather than appearing intermittently, the K-H instability has saturated in a steady state, as seen from the plots of the maximum velocities versus time (Figs. 20*a* and 20*b*). The K-H modes appear as traveling waves, and the resulting toroidal field strengths are thus maintained at fairly constant levels, as can be seen in Figure 20*c*. There is a clear polarity, as indicated by the fact that $|\min B_x|$ is about 5 times larger than $\max B_x$, there are no reversals of polarity, and this behavior

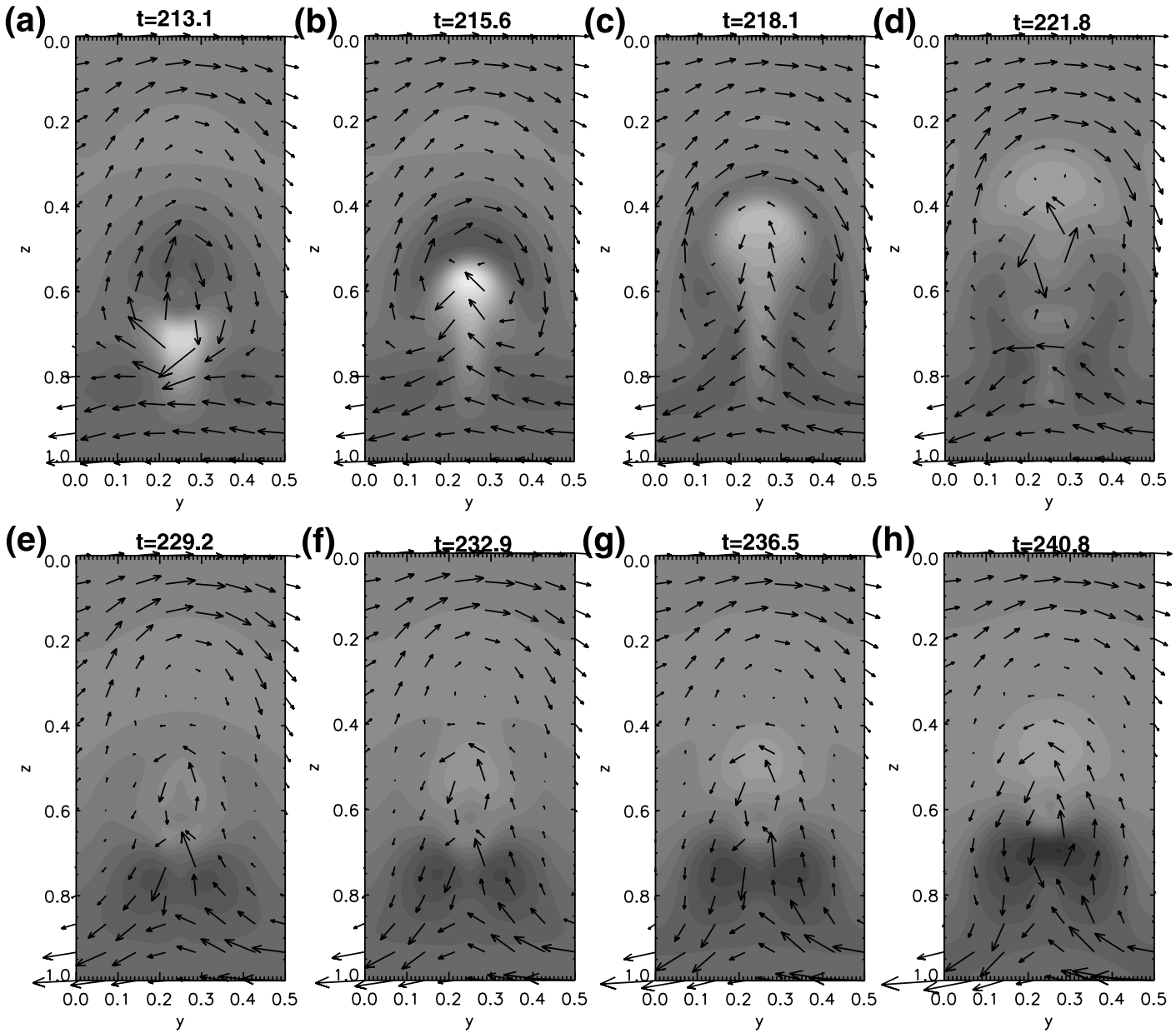

FIG. 15.—Dynamics of a polarity reversal in the system. Shown again are magnetic fields averaged across the x-direction, with poloidal field (B_y, B_z) indicated with arrows and toroidal field B_y with shading (*dark*, positive; *light*, negative) from case A2, but this time for $t = 213.1$–240.8. This process begins when the system produces a very strong negative toroidal structure, and then much of this toroidal field rises buoyantly out of the shear layer (*a*–*c*). The result of this is that the K-H instability produces only the upper poloidal loop (*d*), rather than two as in Fig. 13*e*. The action of rising pulls some of the surrounding positive toroidal field into the lower shear region, which is then twisted into a poloidal loop (*e*, *f*). Together these two clockwise poloidal loops reverse the overall poloidal field in the domain, so a positive toroidal structure now begins to build (*f*–*h*).

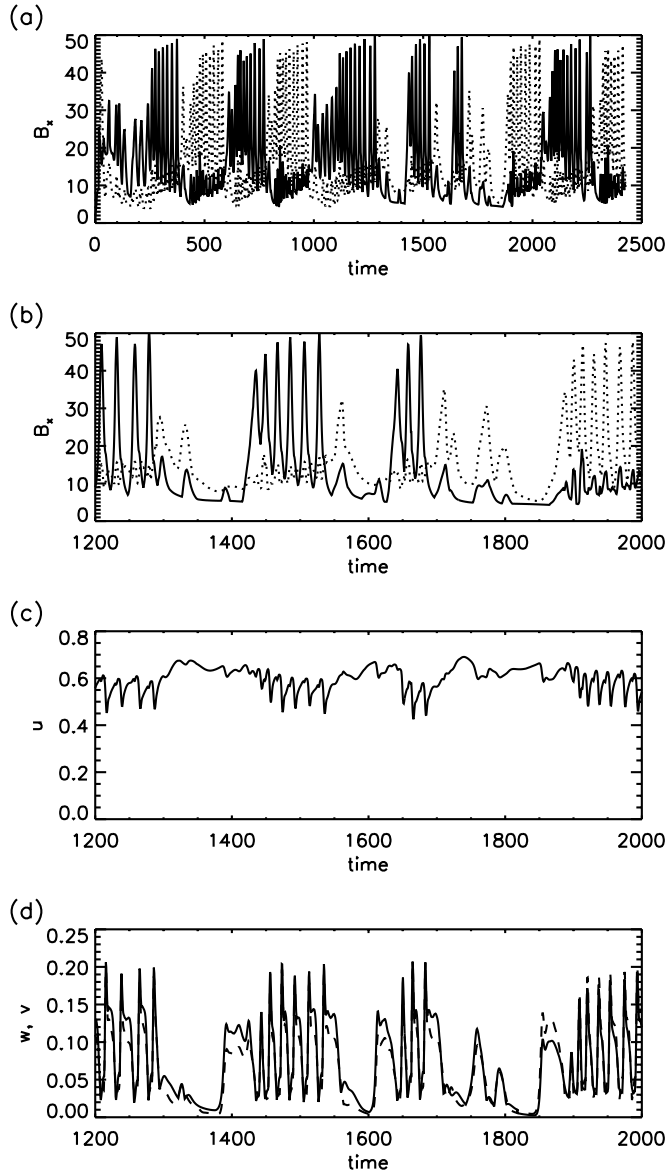

FIG. 16.—Very long time evolution of the system, observed in both magnetic fields and velocity. Plotted are (*a*) the extreme values of B_x for the entire simulation and the peak values of (*b*) the toroidal field and (*c*, *d*) the velocities (*v*, *dashed line*; *u*, *w*, *solid line*), for an interval exhibiting a period of decreased activity. The system operates convincingly as a dynamo for at least 2500 time units. However, evident are three brief periods when the fields are resistively decaying because the K-H modes did not appear (v, w become small). Case A5 is plotted here. This is the same dynamo as case A2 statistically, except that it started from different initial conditions [larger $B_y^2(t=0)$], so the field intensity is scaled differently. For direct comparison with case A2, multiply the magnetic field values by $[a_m(A2)/a_m(A5)]^{1/2} = \sqrt{1000}$.

appears to be stable. This case is another example of the remarkable dynamo properties of this system.

4. DISCUSSION

We have studied the properties of a simple system consisting of a stratified layer of conducting fluid subject to a localized velocity shear. Rather surprisingly, this system is capable of dynamo action. The generation of magnetic field proceeds through a complex sequence of events including the shearing of poloidal field to generate toroidal field, the onset of a K-H type instability that, together with the buoyant rise of the toroidal magnetic structures, regenerates the poloidal field to complete the dynamo cycle. The energy source is the shear, and the dynamo appears to equilibrate with the magnetic energy in equipartition with the kinetic energy, $M_A \approx 1$, using the maximum norm of B_y in the dynamo phase as the measure in equation (15) [rather than the initial field $B_y(t=0)$ used for the values in Table 1].

Magnetic buoyancy plays an essential role in the dynamo mechanism. It is the buoyant steepening of the velocity shear and the buoyant rise of magnetic structures relative to the region of intense shear that allow the dynamo cycle to proceed. This also implies that for initial magnetic fields below a critical strength, the dynamo instability is never triggered, and the magnetic field ultimately decays away. Because the rate of resistive decay depends on the magnetic Reynolds number, the critical initial field strength for dynamo action also depends on Re_m, decreasing as Re_m increases. However, for any finite Re_m the critical field strength for dynamo action remains finite, implying that the dynamo is intrinsically nonlinear and that it cannot be captured by a kinematic treatment.

Variations in Re_m change not only the critical strength for the onset of dynamo action but also the qualitative behavior of the dynamo itself. For moderate values of Re_m, the dynamo operates in a steady state with no discernible emission of magnetic structures out of the shear region. For larger Re_m, the dynamo exhibits cyclic behavior, whereby magnetic structures of a dominant polarity are created in the shear layer and subsequently expelled. The polarity is preserved over several cycles, then eventually reverses. Occasionally, the polarity reversal fails, and the dynamo enters into a dormant phase of reduced activity. Although it may be possible for the dynamo to switch off completely during one of these intervals, this appears to be unlikely, and it has not been observed so far. For still higher Re_m, the dynamo becomes chaotic with no apparent dominant polarity present, and toroidal magnetic structures of both signs are produced almost simultaneously. We conjecture that for higher values of Re_m *and* Re the system will enter into a fully turbulent MHD state, although we have no numerical simulations to support this at this time.

One of the intriguing aspects of this system, above and beyond the fact that it is an efficient dynamo at all, is that it appears to produce magnetic structures with a given twist. This can be seen in Figure 15, which shows the relationship between the poloidal and toroidal magnetic fields. When the polarity of the toroidal structure is negative, the poloidal field above z_v is clockwise (Fig. 15*a*). After a polarity reversal when the toroidal structure becomes positive, the upper poloidal field also reverses to become anticlockwise (Fig. 15*i*). This indicates that there is a fixed relationship between the two components of the field (a "handedness") that is preserved and that the system therefore lacks reflectional symmetry. This property may at first appear strange, since the usual ingredients that lead to a lack of reflectional symmetry, such as rotation, are absent. This lack of reflectional symmetry arises in a subtle manner, through the action of the forcing. The forcing selected here cannot be described solely in terms of a potential function, and thus one of its roles is to induce a certain vorticity distribution. Vorticity, like rotation, is an axial rather than polar vector and is

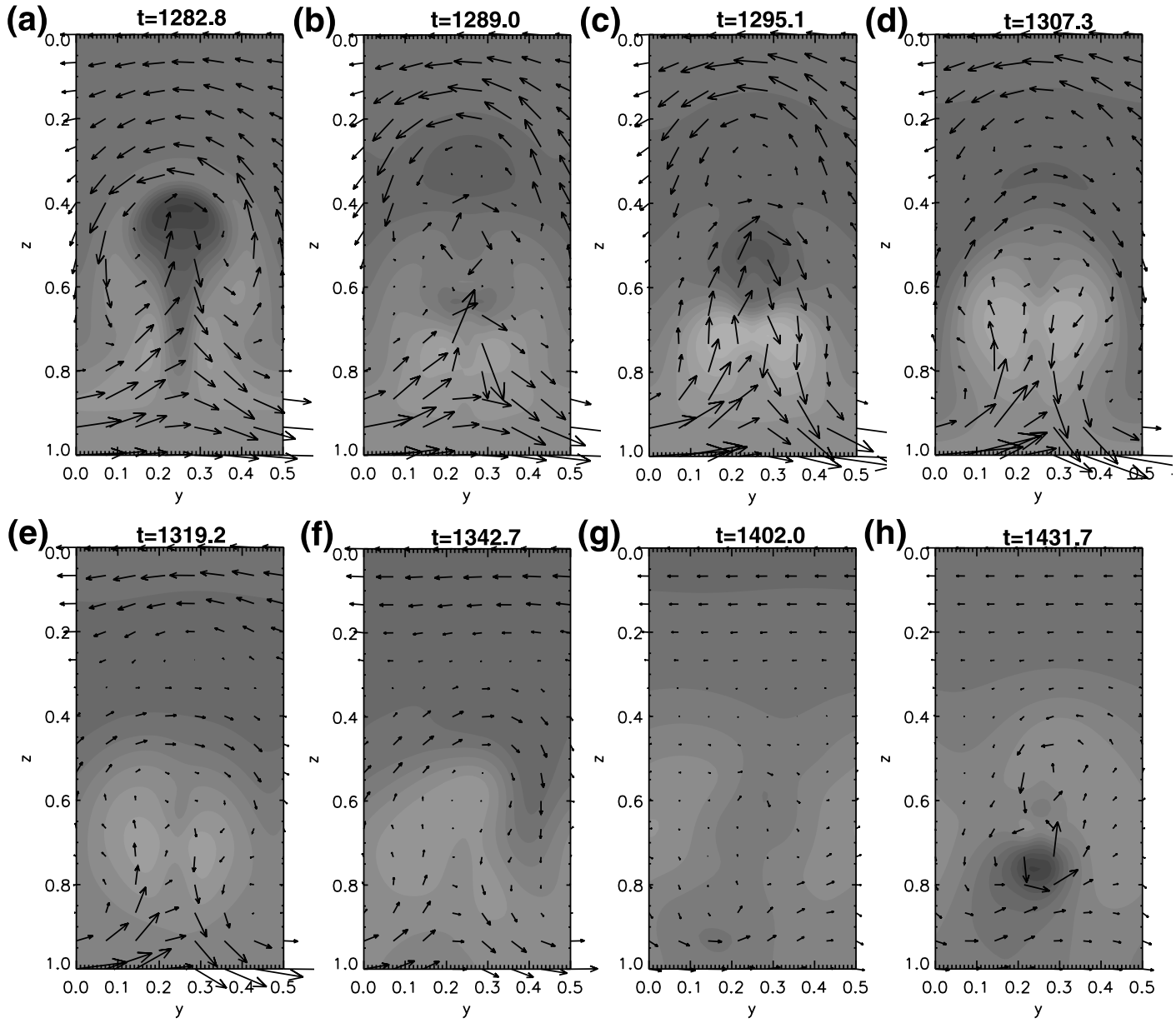

FIG. 17.—Intervals of dynamo inactivity appear to be the result of a failed polarity reversal. Shown again are magnetic fields averaged across the x-direction, with poloidal field (B_y, B_z) indicated with arrows and toroidal field B_y with shading (*dark*, positive; *light*, negative) from case A2, for sequence of times $t = 1282.8$–1431.7. The system starts with a counterclockwise poloidal field that produces a strong positive toroidal structure. This field generates a poloidal flow that advects most of itself out of the shear region, pulling negative field in from the sides (*a*–*c*). However, the resulting clockwise poloidal loops are very weak (*c*) and lead only to the production of a similarly weak negative toroidal structure. This is not strong enough to rise and trigger another K-H instability (*c*–*e*). Fields in the system resistively decay (*e*–*g*) until the very weak remaining poloidal field has sufficient time to build a strong enough toroidal structure (*h*) that can rise and trigger a K-H instability, thus resuming the dynamo cycle.

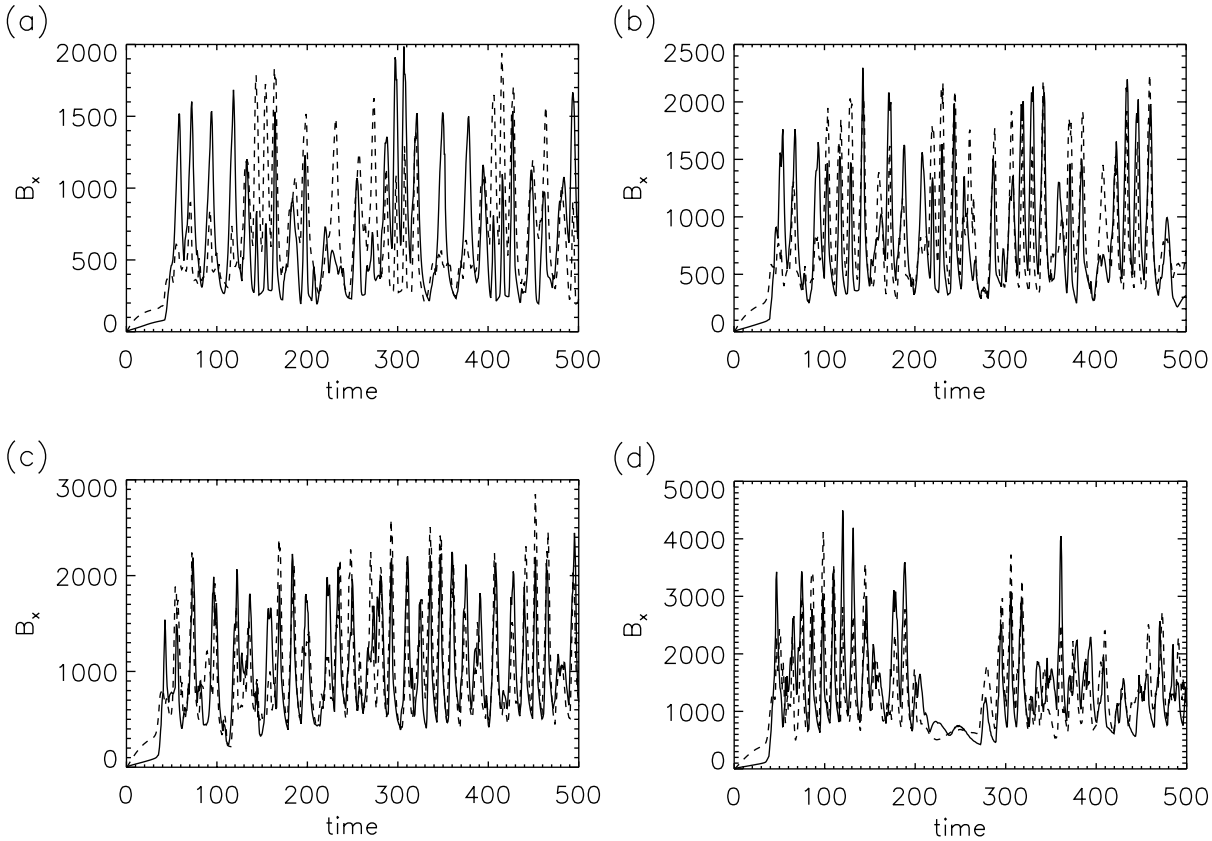

FIG. 18.—Dynamics of the system for various Re_m. Plotted are the extreme values of toroidal field (max B_x, *solid line*; $|\min B_x|$, *dashed line*) for (*a*) case M2 with $\mathrm{Re}_m = 1909$, (*b*) case M3 with $\mathrm{Re}_m = 3820$, (*c*) case M4 with $\mathrm{Re}_m = 7639$, and (*d*) case M5 with $\mathrm{Re}_m = 15,277$. At higher magnetic Reynolds numbers (lower magnetic diffusion), the system no longer shows any well-defined polarity, producing strong peaks in max B_x and $|\min B_x|$ almost simultaneously. The amplitude of these toroidal fields increases with increasing Re_m.

therefore reflectionally antisymmetric, and thus the system as a whole lacks reflectional symmetry.

This property is clearly manifested by the presence of a net kinetic helicity as shown in Figure 21. To understand how this net helicity is generated, note that the strongest toroidal field is necessarily generated in the region of maximum shear in the forced flow $\boldsymbol{U}_0$ and that this is also the region of its strongest vorticity. Upward motions are then generated by magnetic buoyancy there, and thus there exists a strong correlation between negative vertical velocities and the *signed* vorticity (negative for this forcing). The resulting net kinetic helicity may wax and wane as the magnetic fields and the associated flow vary, but it is in general positive for all time. A solution with the opposite net kinetic helicity *cannot* be found for the same forcing. To obtain that other solution, the forcing would have to be changed to induce the reverse shear flow $-\boldsymbol{U}_0$ and thus the opposite-signed vorticity distribution.

Since the phase of the vertical and horizontal K-H modes is tied to the nature of the forced shear, the twist of the magnetic structures is similarly dictated. However, it is important to note that these K-H modes, which create the poloidal magnetic loops and are therefore the key to completing the dynamo cycle, possess no significant kinetic helicity themselves (Fig. 21). The net kinetic helicity of the system, while imprinting a handedness on the system, is merely incidental and not integral to the operation of the dynamo.

Although this system has no Coriolis force, the production of poloidal field by the rise (due to magnetic buoyancy) and twist (due to the K-H instability) is strongly reminiscent of the cyclonic events characterizing the α-effect (a linear relationship between the mean field and the mean electromotive force) in mean field theory. The presence of a helical flow induced by the non–reflectionally symmetric forcing may further suggest that it is useful to interpret the generation of poloidal magnetic field from toroidal in terms of this linear α-effect. However, because the basic regeneration process involves several nonlinear components, there appears to be no simple relationship between the average toroidal electromotive force and the average toroidal field here (Fig. 22). Although we can of course define and compute a value of α by performing a linear regression between these quantities, this α is insufficient to describe the production of poloidal loops since the link between the mean electromotive force and the mean field is so highly nonlinear. This α would have opposite signs above and below the plane of maximum shear, and it would retain a complicated dependence on the mean field in any regime in which the dynamo operated.

In this paper, we have concentrated on the effect of varying Re_m on the system and its dynamo properties. Many other parameters of this problem, such as the Prandtl numbers and the effects of stratification, will affect the operation of the dynamo, and these deserve to be investigated in turn.

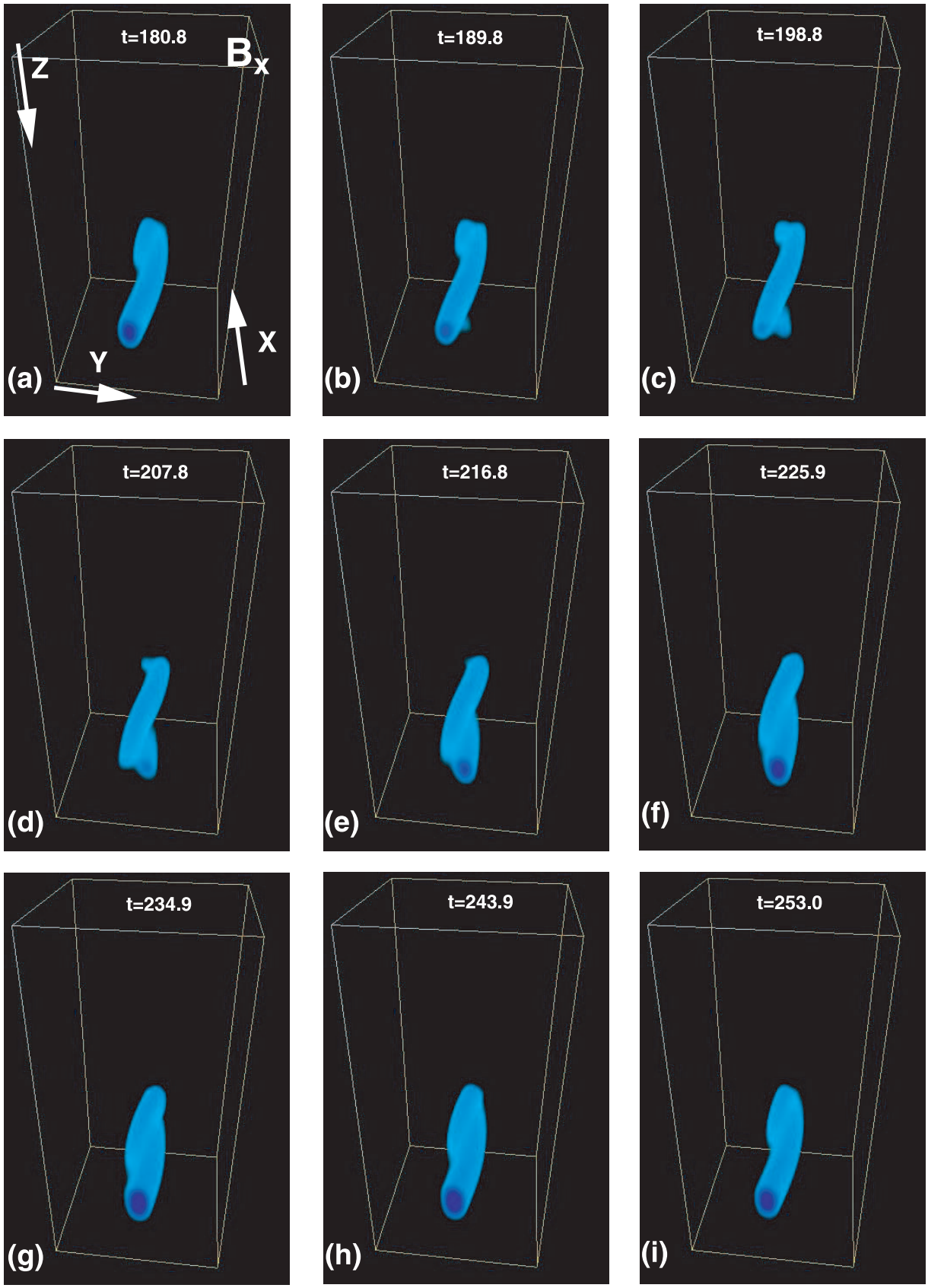

FIG. 19.—Dynamo *without* rising magnetic structures. Shown are volume renderings of B_x from case M6 for a sequence of times $t = 180.8$–253.0. At these parameters, the K-H modes appear as steady traveling waves, causing the magnetic structure to spiral around within the shear layer, without emerging.

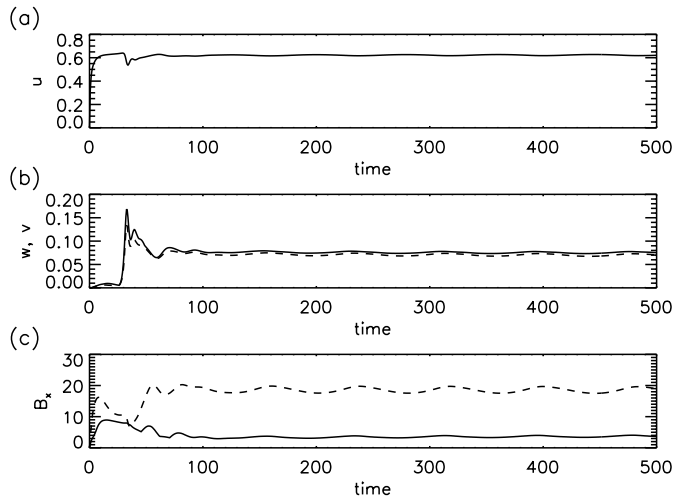

FIG. 20.—Dynamics of the steady dynamo, case M6. Plotted vs. time are the maximum velocities and magnetic fields: (*a*) the toroidal velocity u, (*b*) the poloidal velocities w (*solid line*) and v (*dashed line*), and (*c*) the toroidal field, max B_x (*solid line*) and $|\min B_x|$ (*dashed line*). The buoyancy-induced poloidal flow holds at a fairly steady level rather than appearing in sharp bursts of K-H instability. The dynamo maintains both poloidal and toroidal fields at a steady level, showing a well-defined polarity, with $|\min B_x|$ several times larger than max B_x.

We acknowledge useful discussions with David Hughes and Steve Tobias. Some of this work was carried out while the authors were attending the Solar Magnetism and Related Astrophysics Workshop at the Institute of Theoretical Physics in Santa Barbara, University of California. We thank the staff of the ITP and the organizers of the workshop, George Fisher and Dana Longcope, for their support and interaction. This work was supported by the NASA Solar Physics Supporting Research and Technology grant NAG5-9537. K. S. C. was also supported by a National Science Foundation Graduate Fellowship.

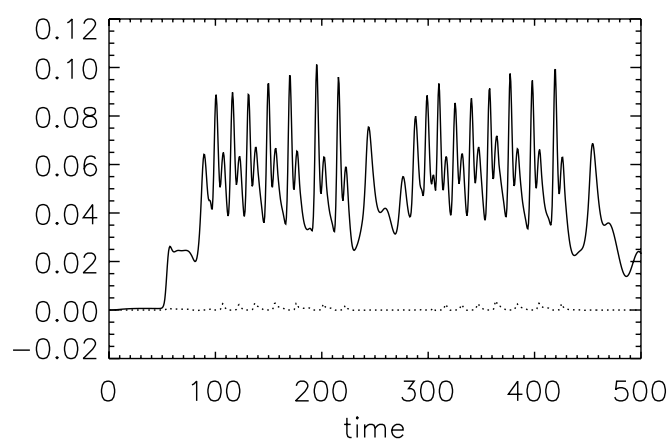

FIG. 21.—Mean kinetic helicity $\langle \boldsymbol{u} \cdot (\nabla \times \boldsymbol{u}) \rangle$ in the system as a function of time for case A2 (*solid line*). Also shown (*dotted line*) is the component of kinetic helicity that is dependent on gradients in the x-direction: $\langle w\partial_x v - v\partial_x w \rangle$. This component represents the kinetic helicity of the K-H modes, since these are the only flows that break the x-invariance of the system, and has little effect on the mean kinetic helicity.

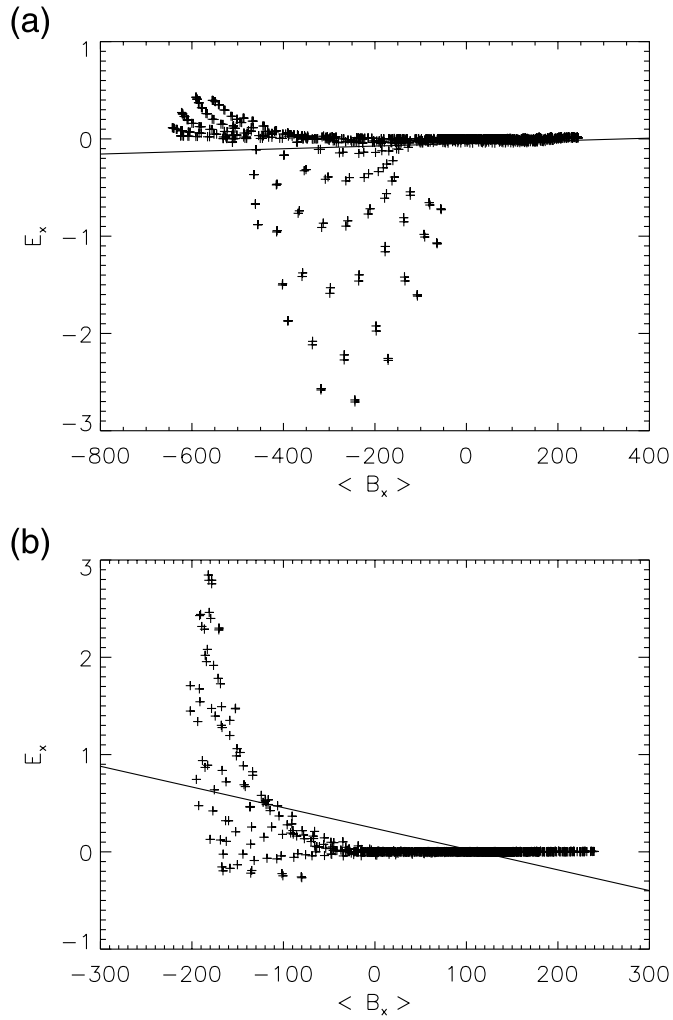

FIG. 22.—Effect of the complex nonlinearity of the system on the relationship between the average electromotive force and the mean field. Plotted is the mean electromotive force in the toroidal direction, $\mathscr{E}_x = (\boldsymbol{u}' \times \boldsymbol{B}') \cdot \hat{\boldsymbol{x}}$ (where dashed variables are fluctuations about the x-average value), against the mean toroidal field, $\langle B_x \rangle$. The plots shown are for case A2 at $t = 119.1$ (during a K-H event), both above the level of maximum shear (depth $z = 0.31$–0.63; *top*) and below ($z = 0.63$–0.95; *bottom*). The overlaid lines indicate the linear regression fits to the points and show that a linear analysis is insufficient.

REFERENCES

Babcock, H. W. 1961, ApJ, 133, 572
Brandenburg, A. 2001, ApJ, 550, 824
Brandenburg, A., & Schmitt, D. 1998, A&A, 338, L55
Brummell, N., Cline, K., & Cattaneo, F. 2002, MNRAS, 329, L73
Cline, K. S., Brummell, N. H., & Cattaneo, F. 2003, ApJ, 588, 630
Defouw, R. J. 1976, ApJ, 209, 266
Dikpati, M., & Gilman, P. 2001, ApJ, 551, 536
Drazin, P. G., & Reid, W. H. 1981, Hydrodynamic Stability (Cambridge: Cambridge Univ. Press)
Ferriz-Mas, A., Schmitt, D., & Schüssler, M. 1994, A&A, 289, 949
Goode, P. R., Dziembowski, W. A., Korzennik, S. G., & Rhodes, E. J. 1991, ApJ, 367, 649
Krause, F., & Rädler, K.-H. 1980, Mean-Field Magnetohydrodynamics and Dynamo Theory (Oxford: Pergamon)
Leighton, R. B. 1969, ApJ, 156, 1
Meneguzzi, M., Frisch, U., & Pouquet, A. 1981, Phys. Rev. Lett., 47, 1060
Moffatt, H. K. 1978, Magnetic Field Generation in Electrically Conducting Fluids (Cambridge: Cambridge Univ. Press)
Moss, D., Tuominen, I., & Brandenburg, A. 1990, A&A, 240, 142
Parker, E. N. 1955a, ApJ, 121, 491
———. 1955b, ApJ, 122, 293
———. 1979, Cosmical Magnetic Fields (Oxford: Clarendon)
Spiegel, E. A. 1972, in Physics of the Solar System, ed. S. I. Rasool (Washington: NASA), 61
Spiegel, E. A., & Zahn, J.-P. 1992, A&A, 265, 106
Spruit, H. C. 1980, A&A, 98, 155
Steenbeck, M., & Krause, F. 1969, Astron. Nachr., 291, 49
Steenbeck, M., Krause, F., & Rädler, K.-H. 1966, Z. Naturforsch, 21a, 369
Thelen, J.-C. 2000, MNRAS, 315, 155
Thompson, M. J., et al. 1996, Science, 272, 1300
Tobias, S. M., Brummell, N. H., Clune, T. L., & Toomre, J. 2001, ApJ, 549, 1183
Weiss, N. O. 1994, in Lectures on Solar and Planetary Dynamos, ed. M. R. E. Proctor & A. D. Gilbert (Cambridge: Cambridge Univ. Press), 59